2021

A Finite Difference Model For Induced Hypothermia During Shock

Dylan S. Lyon
University of Central Florida

A FINITE DIFFERENCE MODEL FOR INDUCED HYPOTHERMIA DURING SHOCK

by

DYLAN S. LYON

A thesis submitted in partial fulfillment of the requirements

for the Honors in the Major Program in Engineering

in the College of Engineering and Computer Science

and in the Burnett Honors College

at the University of Central Florida

Orlando, Florida

Spring Term
2021

Thesis Chair: Dr. Alain J. Kassab

ABSTRACT

The modified Fiala model from Westin was implemented with conditions for circulatory shock and hypothermia. The purpose is to model Emergency Preservation and Resuscitation (EPR), a procedure for inducing hypothermia in patients. Cold tissue temperatures reduce metabolism exponentially, greatly extending the window of anaerobic metabolic activity before permanent deoxygenation damage. EPR in patients undergoing hypovolemic shock can preserve the patient until primary surgical care and blood transfusions are attainable, thereby increasing survival rates. The main applications of EPR are military in-situ stabilization for transit to clinical care and extending the survivability of patients requiring prolonged surgery before blood transfusion. The model explored in this paper seeks to model the tissue temperatures of the body while enduring circulatory shock and various options of cooling devices. Calibrating this model with already available data enables its use for getting preliminary results and design parameters for prototype cooling devices. The final objective of this research is to support the design of a cooling device that can induce sustained hypothermia in a field setting, while still being mobile enough for military and ambulance use.

ACKNOWLEDGMENTS

Many thanks to
Dr. Alain Kassab,
Dr. William Decampli,
and Kyle Beggs
for their guidance and assistance

TABLE OF CONTENTS

LIST OF FIGURES

LIST OF TABLES

INTRODUCTION

Background

Circulatory shock, the condition of having reduced, pulsed, or nonexistent blood circulation, is a life-threatening condition. A patient undergoing circulatory shock is at risk of deoxygenation in affected tissues, which can cause damage in minutes and permanent life-threatening damage in a few minutes more. [1] The imminent damage is caused by cell hypoxia, interrupting metabolic processes and quickly exceeding the anaerobic strain that tissues can undergo. [1] Tissues with more metabolic activity like those in the brain and kidneys are the first to be severely affected. [2]

There are four types of shock, though the purpose of this paper is to treat hypovolemic shock. As the name implies, hypovolemic shock is deoxygenation due to extreme reduction in blood volume. The primary cause of hypovolemic shock is hemorrhage, the loss of blood through ruptured blood vessels. [3] Hypovolemic shock is an effect from amputations, gunshot or stabbing wounds, and vessels ruptured from impacts. This makes treatment of hypovolemic shock a key research area for overtly dangerous professions e.g. military personnel, firefighters, and police officers. [4]

Initial treatment of hypovolemic shock is stemming the blood loss of the patient, usually achieved either by a tourniquet or suture. Stemming blood loss does nothing to restore blood volume, and in most cases a blood transfusion is required. Secondary treatment involves transporting the patient to a hospital or clinic. The patient will undergo a transfusion of either blood or an intravenous crystalloid like saline. [5] Either case will restore circulatory volume, stabilizing the patient's blood circulation provided that the ruptured vessels have already been

resealed. In extreme cases of hypovolemic shock, isotonic saline transfusions will not restore platelet counts and the ruptured vessels will need to be resealed manually. [5]

Transportation to a hospital is an ineffectual method of treatment for hypovolemic shock. The elapsed time from primary treatment to hospital care often exceeds the window of non-permanent deoxygenation damage: A study [6] found that nearly a quarter of combat deaths in Iraq and Afghanistan between 2001 and 2011 were potentially treatable, and yet 90% of the deaths occurred before reaching the nearest medical facility. Current iterations for blood transfusion devices are not easily transported, making field transfusions impractical. [7]

An alternative secondary care method involves induced hypothermia. This method is premised on the van't Hoff Q_{10} Law [8], which states that a decrease in local tissue temperature leads to an exponential decrease in metabolism, and thereby local oxygen consumption and anaerobic metabolic activity. Benefits are only realized at large drops in temperature in order to surpass the body's shivering and warming responses. In extreme cases this can be $20℃$ below thermal neutrality and well within the hypothermia range. [9]

The treatment itself is referred to as Emergency Preservation and Resuscitation, or EPR. [1] After initial treatment of the patient, the patient undergoes induced hypothermia either on-site or during transport to a medical facility. The reduced need for oxygenation greatly extends the survival window until hospital care, up to 60 minutes. [1] Upon arrival the patient undergoes a blood transfusion with blood cooled to a similar temperature as the patient's mean arterial blood temperature, and their cooled tissues are gradually rewarmed.

Induced hypothermia is complicated by the need for in-the-field refrigeration capability. Existing refrigeration devices include blankets, helmets, and injection of cold IV fluids. Any

such device must be able to be carried via vehicle or person while containing enough energy and/or fluid to refrigerate tissues for upwards of 10 minutes in an outdoor setting. This condition has led to targeted EPR devices that focus cooling on select tissues that are the first to sustain permanent deoxygenation damage; Notably, the brain. [10] Successful testing in animal and human subjects suggests that targeted EPR is both effective and has the potential to be applied outside of medical facilities. [11] [12]

The severity of the injury and the risks of EPR limit the experimentation of diverse EPR refrigeration devices on live subjects. Computerized thermoregulatory models of the human body provide an alternative method of evaluating a cooling device's efficacy. Finite difference models like the Fiala model can provide temperature queries in any tissue for a wide range of boundary conditions, including the transient or steady state. [13] By converting cooling devices into the Fiala model's boundary conditions, metrics of a refrigeration device's success like hypothalamic temperature can be recovered at any time query for comparison to clinical trials.

Purpose of Present Study

EPR devices need to be able to cool vulnerable areas of the body to 10℃ within 30 minutes for optimal survival rates. [1] Can the Fiala thermoregulatory model be modified to accurately model the EPR refrigeration process? In order to answer this question, the improved Fiala model from Westin [14] will be implemented. Two devices, a cooling helmet and an ECMO machine, will be applied to the model as transient boundary conditions. Efficacy of the procedure will be measured by central blood pool temperatures and hypothalamic temperatures at various time queries. Accuracy of the model will be validated first against Fiala's steady-state temperature responses [15], and later a cooling helmet [10] and a saline injection [2].

LITERATURE REVIEW

Thermoregulatory Models

[16] PENNES, H. H., "ANALYSIS OF TISSUE AND ARTERIAL BLOOD TEMPERATURES IN THE RESTING HUMAN FOREARM," JOURNAL OF APPLIED PHYSIOLOGY, VOL. 1, 1948, PP. 93–122.

Pennes [16] performed some of the first invasive temperature measurements of the forearm. Measurements were taken on the forearm at varying lengths, depths, and blood flows. From this data, the study regressed coefficients for the bioheat transfer equation (BHTE), commonly referred to as Pennes' Equation,

$$\rho c \frac{\partial T}{\partial t} = \nabla \cdot \left(k \nabla \cdot T \right) + \rho_{bl} c_{bl} w_{bl} \left(T_{bl,a} - T \right) + q_m \tag{1}$$

Where ρ is density, c is specific heat, T is local tissue temperature, k is tissue conductivity, the bl subscript implies properties of local arterial blood, w_{bl} is the capillary perfusion rate of blood into tissues, and q_m is the rate of metabolic heat generation. Pennes' Equation accounts for blood flow as a perfusive system where blood slows in the capillaries in order to transfer heat primarily without convection. The study used the cylindrical form of this equation and applied it to experimental temperature measurements in the forearm with high accuracy even in 1948. Most of the following thermal models use Pennes' Bioheat Transfer Equation as their governing differential equation.

[17] STOLWIJK, J. A. J., "A MATHEMATICAL MODEL OF PHYSIOLOGICAL TEMPERATURE REGULATION IN MAN," NASA TECHNICAL REPORTS, VOL. 1855, AUG. 1971

Stolwijk [17] studied a new resistance-based model for body temperatures. The focus of this study was to recreate the controlling system in temperature regulation. The model is a concentric

cylinder model with different conductivities assigned to each tissue type, and with blood treated as its own tissue in contact with each other tissue type. It is one of the first computerized models for thermoregulation. Its original application was for the space program, so extreme cold temperatures were tested here although their results are theory without a control group.

[13] D. FIALA, K. J. LOMAS AND M. STOHRER, "A COMPUTER MODEL OF HUMAN THERMOREGULATION FOR A WIDE RANGE OF ENVIRONMENTAL CONDITIONS: THE PASSIVE SYSTEM," JOURNAL OF APPLIED PHYSIOLOGY, VOL. 87, NO. 5, 1999.

Fiala et. al. [13] created what would form the modern models of thermoregulation. The Fiala model is a one-dimensional finite-difference model for the body. It consists of spherical and cylindrical elements with various annular-shaped washers. The innovative part of this model is its handling of the blood pool, with a blood pool overlaid over the entire model with a scalable exposure constant w_{bl}, representing blood perfusion rate. The model combined the best of existing models like Wissler's [18] with a relatively high accuracy and low node count (310 for the full body). [13] The Fiala model is the field-recognized standard for thermoregulation, and is the basis for the Universal Thermal Climate Index (UTCI) parameter set. [15]

[10] DIAO, C., ZHU, L., AND WANG, H., "COOLING AND REWARMING FOR BRAIN ISCHEMIA OR INJURY: THEORETICAL ANALYSIS," ANNALS OF BIOMEDICAL ENGINEERING, VOL. 31, 2003, PP. 346–353.

Diao [10] A performed a theoretical study of the efficacy of external SBC with a simple mathematical formulation. The study used a hemisphere model for the brain with 4 tissue layers and a separate blood tissue. Diao [10] also made use of the Q_{10} law proposed by van't Hoff [8] for approximating changes in metabolic heat due to changes in temperature,

$$q = q_0 \cdot Q_{10}^{\left(\frac{T-T_0}{10°C}\right)} \quad (2)$$

Where q is local metabolic heat generation, q_0 is q at thermal neutrality, T is local temperature, and Q_{10} is a tissue-dependent constant that governs the behavior of metabolic heat generation every 10°C and typically lies between 2 and 3. [8] The main result of the study is that external devices such as a cooling helmet or ice held at 0°C are ineffective at inducing brain cooling; The interior of the brain is warmed too profoundly by the carotid artery to have any uniform cooling effect. [10]

[2] KONSTAS, A.-A., NEIMARK, M. A., LAINE, A. F., AND PILE-SPELLMAN, J., "A THEORETICAL MODEL OF SELECTIVE COOLING USING INTRACAROTID COLD SALINE INFUSION IN THE HUMAN BRAIN," JOURNAL OF APPLIED PHYSIOLOGY, VOL. 102, 2007, PP. 1329–1340.

Konstas [2] performed a study of existing trials on brain cooling with a new apparatus. The study used the same hemispherical model of Diao [10] with an isotonic saline injection into the carotid artery. The study showed extreme promise with hypothermia achieved within 10 minutes. The primary differences are the cancellation of the carotid artery's warming effect, the ischemic effect of hemodilution, and the sharp decrease in the capillary perfusion parameter during hemodilution and hypothermia.

[14] J. WESTIN, "AN IMPROVED THERMOREGULATORY MODEL FOR COOLING GARMENT APPLICATIONS WITH TRANSIENT METABOLIC RATES," STARS ELECTRONIC THESES AND DISSERTATIONS, NO. 3704, 2008.

Westin [14] is an implementation of the Fiala model intended to model a full-body liquid cooling garment. This thesis is notable for its advanced treatment and analytical validation at cold

temperatures and at extreme boundary conditions (Forced liquid convection). Further, the Westin model's conversion of skin boundary conditions to a modular fixed heat flux and sweat condition is a necessary step towards modelling external cooling devices. Studies like Diao [10] propose external cooling helmets and blankets without full-body simulation; Westin's modular boundary improvements are invaluable in these modelling scenarios. The implementation of the Fiala model in this current thesis is an implementation of Westin's improved model.

Emergency Preservation and Resuscitation

[4] D. TRUNKEY ET. AL., "ACCIDENTAL AND INTENTIONAL INJURIES ACCOUNT FOR MORE YEARS OF LIFE LOST IN THE U.S. THAN CANCER AND HEART DISEASE. AMONG THE PRESCRIBED REMEDIES ARE IMPROVED PREVENTIVE EFFORTS, SPEEDIER SURGERY AND FURTHER RESEARCH.," SCIENTIFIC AMERICAN, VOL. 249, NO. 2, PP. 28-35, 1983.

Trunkey [4] is the driving paper behind EPR research. This paper recorded the effects of physical injuries that resulted in shock. The study found a trimodal distribution of death times after injury from hypovolemic shock: The first and largest mode, within 60 minutes, due to immediate damage to the brain, spinal cord, and ruptured arteries. The next two modes were low blood volume / lack of access to blood transfusion in ensuing hours, and complications beyond one week after injury. Trunkey [4] led to tremendous funding into treatment in the first 60 minutes after injury, including field treatment.

[11] TISHERMAN, S. A., "SUSPENDED ANIMATION FOR RESUSCITATION FROM EXSANGUINATING HEMORRHAGE," CRITICAL CARE MEDICINE, VOL. 32, 2004.

Tisherman [11] was among the first to carry out EPR in animals with a high success rate. This study was a canine trial at extreme tympanic membrane temperatures (T_{ty}). The method of induced hypothermia is isotonic saline injected into the femoral arteries. The trauma is complete cardiac arrest after controlled hemorrhage from the aorta. After cooling for a predetermined time and temperature, the canines are reperfused and rewarmed via cardiopulmonary bypass. This study showed the promise of EPR as in the case of canines treated for 60-90 minutes of complete cardiac arrest with a resulting T_{ty} of 10°C, profound hypothermia, all of the canines were revived to be physically and histologically normal. The study showed sustained disabilities in the case of partial hypothermia treatments and long hypothermia treatments of 120 minutes or more. The risk in short treatments was that the benefits of reduced metabolism are not realized and the flushing of blood promotes deoxygenation. The risks of long cold exposure include denaturing of enzymes and damages to organ tissues, including a case of coma. The study also tried limited tests of 14 different drugs intended to relieve side effects of the procedure. The antioxidant Tempol showed promise in reducing the clotting of arteries and subsequent infarction during the procedure.

[7] E. KAGAWA, "EXTRACORPOREAL CARDIOPULMONARY RESUSCITATION FOR ADULT CARDIAC ARREST PATIENTS," WORLD JOURNAL OF CRITICAL CARE MEDICINE, VOL. 1, NO. 2, PP. 46-49, 2012.

Kagawa [7] investigates the effect of using an ECMO machine on cardiac arrest patients. The paper connects wean times, mass flow rates, and an initial isotonic saline circuit in the ECMO machine together. It also attests to the findings of Kim [19] that even brief injections of isotonic saline prior to full ECMO catheterization can reduce temperatures by as much as 1.14℃.

Kagawa also provides a volumetric bound for mobile ECMO device saline capacities until closed blood circulation.

[1] S. A. TISHERMAN, M. E. KUTCHER AND R. M. FORSYTHE, "EMERGENCY PRESERVATION AND RESUSCITATION FOR CARDIAC ARREST FROM TRAUMA," INTERNATIONAL JOURNAL OF SURGERY, VOL. 33B, PP. 209-212, 2016.

Tisherman [1] is an introduction to EPR and a description of an ongoing (2020) clinical trial in a hospital setting. The results have yet to be published, but news reports have reported on successful cases in the trial including successes after complete cardiac arrest. [12] The report further details that the necessary levels of hypothermia at $10℃ - 15℃$ were achieved in the trial. Another important detail of the approved trial was that the trial attained approval without prior patient consent, the first step to becoming a widely-practiced procedure on incapacitated patients. [12] Tisherman [1] is an excellent introduction to the basis of EPR for the unacquainted, and has experimental correlations for oxygen consumption per metabolism, a possible future direction for the current paper's Fiala model.

METHODS

Cooling Devices

Two different cooling devices will be considered in this paper for validation.

The first is the cooling helmet from Diao et al. [10] The cooling mechanism is a close-fitting helmet that covers the patient's head (The "head" element in the model). It is modeled by a fixed convection constant $h_{sk} = 30\ (W/m^2K)$ that replaces all convection U in that element. The surrounding temperature T_{air} is replaced with the helmet's effective temperature T_{device}, taken to be 0℃. This will be used for validation, despite the study showing that this device did not reach the required cooling for EPR. [10]

The second device is a modified Extracorporeal Membrane Oxygenation (ECMO) machine. ECMO machines are used to oxygenate blood during periods of heart, lung, or circulatory failure. ECMO machines are the operative device in cardiopulmonary bypass, which consists of a pump pulling deoxygenated blood from a vein, oxygenating the blood, and then returning the blood to an artery (or arteries) with an additional force to emulate nominal blood pressure. [20]

The particular ECMO machine used in this study consist of drawing blood from the vena cava and injecting the oxygenated blood into the carotid artery bifurcation. [2] This study is an emulation of Konstas [2], with the modified Fiala model in place of the brain-only model from Konstas. The blood can be pre-cooled by the ECMO machine to have any achievable outlet temperature. The study from Konstas [2] also accounts for an isotonic saline injection with the ECMO outflow in the carotids as part of its cooling method; This configuration will also be used for validation.

Modified Fiala Model

The Fiala model [13] is a finite-difference transient thermoregulatory model with passive and active systems. The model consists of 11 solid elements representing large body parts. The head is modeled by a sphere, and the rest of the elements are modeled as cylinders. Arterial blood is modeled by an isothermal single-node element termed the Central Blood Pool (CBP), in perfusive (volumetric) contact with all other elements of the body. Parameters for the Fiala model used in this study are located in Appendix A.

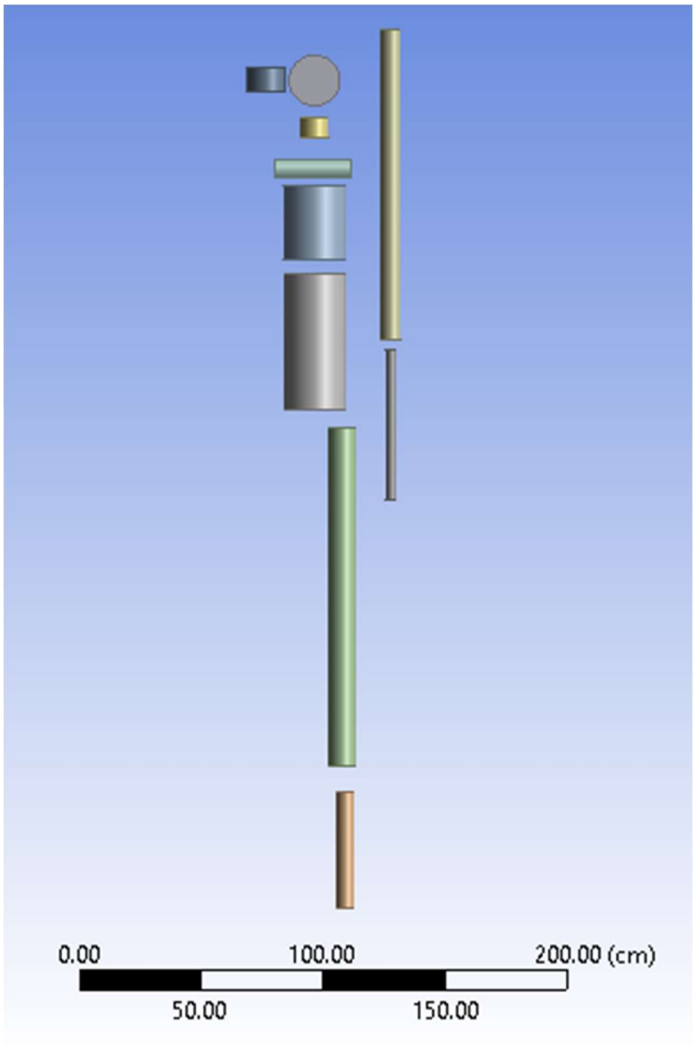

Figure 1 - Fiala Model whole-body structure

Each element besides the CBP is subdivided into angular segments called sectors. These sectors have differing interior angles ϕ and view factors ψ that affect local convection due to restricted airflow (e.g. flow between the legs). Only the radial direction is modeled, so there is no conductive contact between adjacent sectors. Each element besides the CBP is also subdivided into radial segments called washers. For cylindrical elements, washers are concentric hollow cylinders; For spheres, washers are concentric hollow shells. Each washer has constant thermophysical parameters and constant density, allowing each washer to be modeled by a single temperature node. The first washer in every element is called the core element, and it is in conductive contact with the second washer in every sector. The core element, despite having disparate points of contact with each sector in the element, is assumed to be isothermal to maintain radial symmetry about $r = 0$. Below is an example cross section of the arm, a cylindrical element with 3 sectors and 16 washers. The central washer is the arm bone tissue, and the outer washers in the 3 sectors represent muscle, fat, and skin tissues.

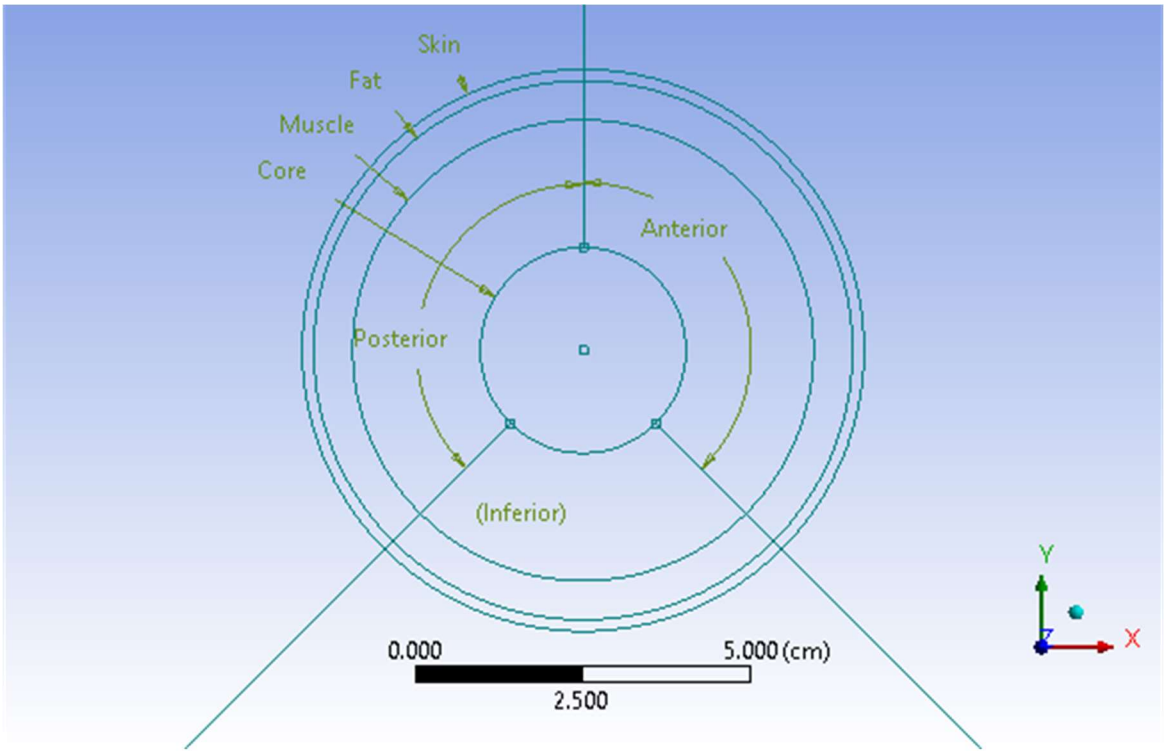

Figure 2 – Arm element cross-section

The governing differential equation in the Fiala model is the one-dimensional Pennes Bioheat Equation [16] with constant thermal conductivity k; in polar coordinates it is

$$k\left(\frac{\partial^2 T}{\partial r^2}+\frac{\omega}{r}\frac{\partial T}{\partial r}\right)+\beta\left(T_{bl,a}-T\right)+q_m=\rho c\frac{\partial T}{\partial t} \tag{3}$$

where k, ρ, and c have their usual definitions, ω is a shape parameter which is 1 for cylindrical elements and 2 for spherical elements, r is the radius from the center of the core washer, β is the blood perfusion factor, $T_{bl,a}$ is the temperature of the arterial blood, and q_m is metabolic heat generation per unit volume. [16]

In the Westin [14] execution of the Fiala model a Crank-Nicholson discretization scheme is used. Crank-Nicholson averages implicit and explicit schemes to generate a new temperature vector at each timestep.

The implicit operator for Pennes (2) for temperature at washer node r at time t is

$$\begin{aligned}\Omega_{implicit}T_r &= \rho_r c_r \frac{T_r^{(t+1)} - T_r^{(t)}}{\Delta t} \\ &= k_r \left[\frac{T_{r+1}^{(t+1)} - 2T_r^{(t+1)} + T_{r+1}^{(t+1)}}{\Delta r^2} + \omega \frac{T_{r+1}^{(t+1)} - T_{r-1}^{(t+1)}}{2r\Delta r} \right] + q_{m,r}^{(t+1)} + \beta_r^{(t+1)} \left[T_{bl,a}^{(t+1)} - T_r^{(t+1)} \right]\end{aligned} \tag{4}$$

The explicit operator for Pennes (2) for temperature at washer node r at time t is

$$\begin{aligned}\Omega_{\exp licit}T_r &= \rho_r c_r \frac{T_r^{(t+1)} - T_r^{(t)}}{\Delta t} \\ &= k_r \left[\frac{T_{r+1}^{(t)} - 2T_r^{(t)} + T_{r+1}^{(t)}}{\Delta r^2} + \omega \frac{T_{r+1}^{(t)} - T_{r-1}^{(t)}}{2r\Delta r} \right] + q_{m,r}^{(t)} + \beta_r^{(t)} \left[T_{bl,a}^{(t)} - T_r^{(t)} \right]\end{aligned} \tag{5}$$

Averaging the two equations and separating future temperatures from present temperatures leaves the final discretized form

$$\begin{aligned}&\left(\gamma_r - 1\right) T_{r-1}^{(t+1)} + \left[\frac{\zeta_r}{\Delta t} + 2 + \delta_r \beta_r^{(t+1)} \right] T_r^{(t+1)} - \left(1 + \gamma_r\right) T_{r+1}^{(t+1)} - \delta_r \beta_r^{(t+1)} T_{bl,a}^{(t+1)} \\ &= \\ &\left(1 - \gamma_r\right) T_{r-1}^{(t)} + \left[\frac{\zeta_r}{\Delta t} - 2 - \delta_r \beta_r^{(t)} \right] T_r^{(t)} + \left(1 + \gamma_r\right) T_{r+1}^{(t)} + \delta_r \beta_r^{(t)} T_{bl,a}^{(t)} + \delta_r \left[q_{m,r}^{(t)} + q_{m,r}^{(t+1)} \right]\end{aligned} \tag{6}$$

where

$$\gamma_r = \frac{\omega \Delta r}{2r} \tag{7}$$

$$\delta_r = \frac{\Delta r^2}{k_r} \tag{8}$$

$$\zeta_r = 2\Delta r^2 \frac{\rho_r c_r}{k_r} \tag{9}$$

and Δr is the spacing between washers of constant radius and Δt is a user-specified timestep that is sufficiently small for numerical stability. Handling of exceptions in the form of skin nodes,

core nodes, changing Δr and thermophysical constants, will be addressed below. Boundary conditions with heat like respiration and shivering can all be combined into the q_m terms. Future terms besides the temperature (β^{t+1} and q_m^{t+1}) are computed via an explicit backward finite difference of their present and past values.

Exception 1 – Non-constant Thermal Parameters and Node Spacing

Washers that are in contact but represent two different tissue types have different k, ρ, and c values and often different node spacing. This condition is rectified by adding the condition that heat flux between the nodes must be equal when computed separately at each node for energy to be conserved. When paired with the physical condition that the interpolated interface temperature T_{ifc} is equal when computed from the temperature gradients of both nodes, changing thermophysical parameters and node spacing can be resolved. In this case, the node r is transmitting heat to a fictional node $(r+1)''$ and the node $(r+1)$ is transmitting heat backwards to a fictional node r'', where the superscript $''$ indicates fictional nodes. An example is shown below for two nodes in contact.

Figure. Fictional node contact

The final form of this equation is

$$\begin{aligned}\left(\gamma_r-1\right)A_{B,r-1}T_{r-1}^{(t+1)}+\left[\left(\gamma_r-1\right)A_{B,r}+\frac{\zeta_r}{\Delta t}+2+\delta_r\beta_r^{(t+1)}-(1+\gamma_r)A_{F,r}\right]T_r^{(t+1)}-\left(1+\gamma_r\right)A_{F,r+1}T_{r+1}^{(t+1)}\\ -\delta_r\beta_r^{(t+1)}T_{bl,a}^{(t+1)}\\ =\\ \left(1-\gamma_r\right)A_{B,r-1}T_{r-1}^{(t)}+\left[\left(1-\gamma_r\right)A_{B,r}+\frac{\zeta_r}{\Delta t}-2-\delta_r\beta_r^{(t)}+(1+\gamma_r)A_{F,r}\right]T_r^{(t)}+\left(1+\gamma_r\right)A_{F,r+1}T_{r+1}^{(t)}\\ +\delta_r\beta_r^{(t)}T_{bl,a}^{(t)}+\delta_r\left[q_{m,r}^{(t)}+q_{m,r}^{(t+1)}\right]\end{aligned} \tag{10}$$

Where the A are dimensionless coefficients that account for changes in thermal parameters and spacing (In homogenous tissue (Constant thermal parameters, constant Δr) $A_{B,r-1} = 1$, $A_{B,r} = 0$, $A_{F,r} = 0$, and $A_{F,r+1} = 1$, and equation (10) reduces to equation (6). This equation can thereby be used in homogenous tissue with no consequence, and is thus applied to both homogenous and heterogenous tissues.

Exception 2 – Core Nodes

Core nodes are an exception in that they are in contact with multiple nodes and do not have a backwards node $(r-1)$. The condition applied to the core node is that the sum of the heat fluxes into the core node via conduction with core-adjacent is equal to the sum of the heat fluxes out of the core-adjacent nodes. The new version of Pennes' Equation for the core node is written

$$-\frac{\kappa}{r_{ifc}}\frac{\sum_{s}^{\text{sectors}}\phi_s q_{ifc,s}}{\sum_{s}^{\text{sectors}}\phi_s}+\beta_{iso}\left(T_{bl,a}-T_{core}\right)+q_{m,core}=\rho_{core}c_{core}\frac{\partial T_{core}}{\partial t} \tag{11}$$

Where κ is a geometry constant ($\kappa = 2$ for cylinders, $\kappa = 3$ for spheres), r_{ifc} is the outer radius of the core washer, and $q_{ifc,s}$ is the heat flux between the core node and sector s. A new coefficient θ is introduced to weight the A_F coefficients such that the heat energy continuity is maintained at the interface.

The final form of the core node equation is

$$\left[\frac{\zeta_r}{\Delta t}+\delta_r\beta_r^{(t+1)}+\theta(1-A_{F,r})\sum_{s}^{\text{sectors}}\phi_s\right]T_r^{(t+1)}-\theta A_{F,r+1}\sum_{s}^{\text{sectors}}\phi_s T_{r+1,s}^{(t+1)}-\delta_r\beta_r^{(t+1)}T_{bl,a}^{(t+1)}$$
$$=$$
$$\left[\frac{\zeta_r}{\Delta t}-\delta_r\beta_r^{(t)}+\theta(A_{F,r}-1)\sum_{s}^{\text{sectors}}\phi_s\right]T_r^{(t)}+\theta A_{F,r+1}\sum_{s}^{\text{sectors}}\phi_s T_{r+1,s}^{(t)}+\delta_r\beta_r^{(t)}T_{bl,a}^{(t)}+\delta_r\left[q_{m,r}^{(t)}+q_{m,r}^{(t+1)}\right] \tag{12}$$

Where ϕ_s is the interior angle of sector s, node $(r+1), s$ is the second washer in sector s, and θ is a constant in rad^{-1} (See Appendix B for values).

Exception 3 – Skin Surface Nodes

Skin surface nodes are unique in that they have no forward node $(r+1)$. Rather, a transient heat flux boundary condition is applied at the skin surface. This condition is maintained with a fictional $(r+1)''$ node similar to the Exception 1 case, this time with constant thermal parameters and nodal spacing. The skin heat flux q_{sk}'' is a function of convective heat transfer, radiative heat transfer, and sweating; Details are provided in the skin section of this study. Equating the boundary heat flux with conductive heat at the skin element gives

$$q_{sk}'' = \frac{k_r\left(T_r - T_{(r+1)''}\right)}{r_{sk}\ln\left(\frac{r_{(r+1)''}}{r_r}\right)} \tag{13}$$

Substituting $T_{(r+1)''}$ into the discretized Pennes' Equation for internal nodes gives

$$\begin{aligned}\left(\gamma_r - 1\right)A_{B,r-1}T_{r-1}^{(t+1)} + \left[\left(\gamma_r - 1\right)A_{B,r} + \frac{\zeta_r}{\Delta t} + 2 + \delta_r\beta_r^{(t+1)} - \left(1+\gamma_r\right)A_{F,sk}\right]T_r^{(t+1)} \\ -\left(1+\gamma_r\right)A_{F,r+1}T_{(r+1)''}^{(t+1)} - \delta_r\beta_r^{(t+1)}T_{bl,a}^{(t+1)} \\ = \\ \left(1-\gamma_r\right)A_{B,r-1}T_{r-1}^{(t)} + \left[\left(1-\gamma_r\right)A_{B,r} + \frac{\zeta_r}{\Delta t} - 2 - \delta_r\beta_r^{(t)} + \left(1+\gamma_r\right)A_{F,sk}\right]T_r^{(t)} \\ +\left(1+\gamma_r\right)A_{F,r+1}T_{(r+1)''}^{(t)} + \delta_r\left[q_{m,r}^{(t)} + q_{m,r}^{(t+1)}\right] + \delta_r\beta_r^{(t)}T_{bl,a}^{(t)}\end{aligned} \tag{14}$$

Passive System

The passive system concerns heat fluxes into the body from the environment and changes in heat generation that do not change with respect to temperature error signals from the mind.

Metabolism

Metabolism in the discretized Pennes' Equation is a single variable q_m in W/m^3, which is the addition of several sources:

$$q_m = q_{m,0} + \Delta q_{m,0} + \Delta q_{m,sh} + \Delta q_{m,w,j} + \Delta q_{resp} \tag{15}$$

Where $q_{m,0}$ is the basal metabolic heat rate, $\Delta q_{m,0}$ is the change in metabolic heat generation due to the Q_{10} Law, $\Delta q_{m,sh}$ is the change in metabolism due to the shivering of muscle tissue (See active system section), $\Delta q_{m,w,j}$ is the metabolism due to external work in muscle tissue, and Δq_{resp} is the heat exchange in nodes exposed to the respiratory system.

$\Delta q_{m,0}$ - Q_{10} *Law*

The change in $q_{m,10}$ is premised on the Q_{10} Law from van't Hoff [8] :

$$q = q_{m,0} \cdot Q_{10}^{\left(\frac{T-T_0}{10°C}\right)} \tag{16}$$

where q is the metabolic heat rate per unit volume, $q_{m,0}$ is the basal metabolic heat rate at temperature T_0, T is the current temperature of the tissue, and T_0 is the thermally-neutral temperature of the tissue. The value Q_{10} is a dimensionless constant, between 2 and 3 depending on the amount of activity in the tissue. [8] For the purposes of this study, Q_{10} is assumed to be 2.

The Q_{10} Law in terms of $\Delta q_{m,0}$ is therefore written

$$q_{m,0} + \Delta q_{m,0} = q_{m,0} \cdot 2^{\left(\frac{T-T_0}{10°C}\right)} \tag{17}$$

T_0 is obtained at each node by running the steady-state version of this model without any cooling apparatus and by setting the $\Delta q_{m,0}$ term to 0, thereby negating the effect of the Q_{10} law on its own parameters. Solving the above equation for $\Delta q_{m,0}$ gives

$$\Delta q_{m,0} = q_{m,0}\left(2^{\left(\frac{T-T_0}{10°C}\right)} - 1\right) \tag{18}$$

$\Delta q_{m,sh}$ - *Metabolism due to Shivering*

The metabolism in a muscle-tissue node due to shivering is given as

$$\Delta q_{m,sh} = \frac{a_{sh,j}}{V_{msc,j}} \cdot Sh \tag{19}$$

Where $a_{sh,j}$ is the portion of the muscle shivering load supported by body element j, $V_{msc,j}$ is the total muscle volume in element j in m^3, and Sh is the body-wide shivering output (See active system section) in Watts.

$\Delta q_{m,w}$ - *Metabolism due to Work Inefficiencies*

The metabolism due to work inefficiencies in muscle tissue is given as a function of the whole-body work heat load

$$H = M\left(1-\eta_w\right) - M_0 \tag{20}$$

Where M is the whole-body metabolic rate in Watts, M_0 is the basal metabolic rate in Watts, and η_w is the work efficiency. η_w is given as $0.05 W/W$ at activity values below $1.6 act$, and given by [13] as

$$\eta_w = 0.2\tanh\left(b_1 \cdot act + b_0\right) \tag{21}$$

for $act \geq 1.6$, where the b_0 (-) and b_1 (met^{-1}) are numerical constants (See Table 2 in Appendix A). The specific metabolic heat due to H in body element j is

$$q_{m,w,j} = \frac{a_{m,w,j}}{V_{msc,j}} \cdot H \tag{22}$$

Where $a_{m,w,j}$ is the portion of the muscle work load supported by body element j and $V_{msc,j}$ is the total muscle volume in element j in m^3. The factor $a_{m,w,j}$ varies greatly between elements

for different types of exercise; This effect is negated by assuming the body is sedentary and inactive.

Δq_{resp} – Metabolism due to Respiration

Net heat loss due to respiration is calculated from ambient air conditions T_{air} in ℃ and partial vapor pressure P_{air} in Pascals and the metabolic heat rate M in Watts in the correlation from Fanger [21]

$$\begin{aligned} Q_{resp} &= 3.45M \cdot (0.028 + 6.5\times10^{-5} T_{air} - 4.98\times10^{-6} P_{air}) \\ &\quad +1.44\times10^{-3} M \cdot (32.6 - 0.934 T_{air} + 1.99\times10^{-4} P_{air}) \end{aligned} \tag{23}$$

This total heat flux is imparted as a specific heat generation over the washers that would be exposed to the respiratory tract, via the equation

$$\Delta q_{resp} = -\frac{a_{resp}}{V_{washer}} Q_{resp} \tag{24}$$

Where a_{resp} is the distribution factor for each exposed washer and V_{washer} is the volume of the exposed washer. The distribution factor a_{resp} is 0.25 for outer face muscle, 0.2 for the inner face muscle, 0.25 for the neck muscle, and 0.3 for the lung washer (Core washer of the thorax), such that the sum of $a_{resp} = 1$.

Blood Element

The central blood pool element is a single-node, and therefore isothermal, element. It has one temperature value $T_{bl,p}$ although the arterial blood temperature $T_{bl,a,j}$ that reaches a body element j can be directly calculated from $T_{bl,p}$ via

$$T_{bl,a,j} = \frac{T_{bl,p}\sum_{r}^{nodes}\beta_r V_r}{h_x + \sum_{r}^{nodes}\beta_r V_r} + \frac{h_x \dfrac{\sum_{r}^{nodes} T_r \beta_r V_r}{\sum_{r}^{nodes}\beta_r V_r}}{h_x + \sum_{r}^{nodes}\beta_r V_r} \tag{25}$$

Where h_x is the countercurrent heat exchange coefficient for element j (See Table 4 in Appendix A).

The value of $T_{bl,p}$ is calculated as an average of the body elements' exposure to the blood pool times their tissue temperatures over the total exposure of the body. Note that this puts the central blood pool at timestep t in perfusive contact with the central blood pool at timestep $t+1$, so the previous value of $T_{bl,p}$ lags into future values. This phenomenon is described by the Coupling Coefficient $CplC$, given below.

$$T_{bl,p} = \frac{\sum_{j}^{element}\left[\dfrac{\sum_{r}^{nodes}\beta_{j,r}V_{j,r}}{h_{x,j}+\sum_{r}^{nodes}\beta_{j,r}V_{j,r}} \times \sum_{r}^{nodes} T_{j,r}\beta_{j,r}V_{j,r}\right]}{\sum_{j}^{element}\left[\dfrac{\left(\sum_{r}^{nodes}\beta_{j,r}V_{j,r}\right)^2}{h_{x,j}+\sum_{r}^{nodes}\beta_{j,r}V_{j,r}}\right]} \tag{26}$$

$$CplC = -\sum_{j}^{element}\left[\frac{\left(\sum_{r}^{nodes}\beta_{j,r}^{(t+1)}V_{j,r}\right)^2}{h_{x,j}+\sum_{r}^{nodes}\beta_{j,r}^{(t+1)}V_{j,r}}\right] \tag{27}$$

β_r is the blood perfusion rate factor in node r, analogous to $1/\alpha$ in conduction systems. It is not a constant tissue property and is described by the equation from Westin [14]

$$\beta_r = \beta_{0,r} + \Delta\beta_r \tag{28}$$

Where $\beta_{0,r}$ is the base perfusion rate factor $\beta_{r,0} = \rho_{bl} c_{bl} w_{bl,0,r}$. $\Delta\beta_r$ is the effective change in perfusion rate factor due to metabolic activity $\Delta\beta_r = \mu \Delta q_{m,r}$ where μ is a constant $\mu = 0.932 K^{-1}$ [17] and $\Delta q_{m,r}$ is the change in metabolic heat generation from basal $\Delta q_{m,r} = \Delta q_{m,0} + \Delta q_{m,sh} + \Delta q_{m,w,j}$.

Active System

The active system is a series of signal-activated responses to regulate body temperature in conditions beyond the homeostatic range. The error signals are the error in skin mean temperature $\Delta T_{sk,m}$ in Kelvin, the error in Hypothalamic temperature ΔT_{hy} in Kelvin, and the time derivative of the error of the skin mean temperature $\frac{d\Delta T_{sk,m}}{dt}$ in Kelvin/hour. $\Delta T_{sk,m}$ and ΔT_{hy} are computed with regard to their values at the thermal neutrality temperature vector T_0. $\frac{d\Delta T_{sk,m}}{dt}$ is computed via a backwards finite difference

$$\frac{d\Delta T_{sk,m}}{dt} = \frac{T_{sk,m}^{(t)} - T_{sk,m}^{(t-1)}}{\Delta t} \tag{29}$$

T_{hy} is assumed to be the same temperature as the center of the brain (Core head washer). $T_{sk,m}$ is calculated by averaging the outermost washer temperature $T_{sk,j,s}$ at every sector s of every element j weighted by the area of exposure $A_{sk,j,s}$ and the skin sensitivity $a_{sk,j}$ for element j (See Table 6 in Appendix A)

$$T_{sk,m} = \sum_{j}^{element} \left(a_{sk,j} \sum_{s}^{\text{sector}} \frac{A_{sk,j,s}}{A_{sk,j}} T_{sk,j,s} \right) \tag{30}$$

In response to these 3 error signals, the body produces 4 primary thermoregulatory response signals: Shivering (Sh, in Watts); Vasoconstriction (Cs, dimensionless); Vasodilation (Dl, in Watts/Kelvin); and Sweating (Sw, in grams/minute). [22]

$$Sh = 10\left[\tanh\left(0.48\Delta T_{sk,m} + 3.62\right) - 1\right]\Delta T_{sk,m} - 27.9\Delta T_{hy} + 1.7\Delta T_{sk,m}\frac{dT_{sk,m}}{dt} - 28.6 \tag{31}$$

$$Cs = 35\left[\tanh\left(0.34\Delta T_{sk,m} + 1.07\right) - 1\right]\Delta T_{sk,m} + 3.9\Delta T_{sk,m}\frac{dT_{sk,m}}{dt} \tag{32}$$

$$Dl = 21\left[\tanh\left(0.79\Delta T_{sk,m} - 0.70\right) + 1\right]\Delta T_{sk,m} + 32\left[\tanh\left(3.29\Delta T_{sk,m} - 1.46\right) + 1\right]\Delta T_{hy} \tag{33}$$

$$Sw = \left[0.8\tanh\left(0.59\Delta T_{sk,m} - 0.19\right) + 1.2\right]\Delta T_{sk,m} + \left[5.7\tanh\left(1.98\Delta T_{hy} - 1.03\right) + 6.3\right]\Delta T_{hy} \tag{34}$$

There exist discrete limits on the error signals and thermoregulatory signals, explored extensively in Fiala et. al [22]. In equation (32) for vasoconstriction, the error signal product $\Delta T_{sk,m} \cdot \frac{d\Delta T_{sk,m}}{dt}$ is nonzero only when both $\Delta T_{sk,m}$ and $\frac{d\Delta T_{sk,m}}{dt}$ are negative. This does not apply to the same product when computing Sh in equation (31). The thermoregulatory signal Sh has a maximum value of $350W$, and the signal Sw has a maximum value of 30 grams/minute.

The shivering response is implemented as a change in the metabolic heat rate in the muscle tissue, as described in the passive section. The sweat response is distributed across the body, weighted by the relative area of exposure of section s, $A_{sk,j,s}$ to the area of element j, $A_{sk,j}$; and the skin sensitivity $a_{sw,j}$ for element j (See Table 5 - Distribution Parameters (a) Table 5 in Appendix A)

$$\frac{dm_{sw,s}}{dt} = a_{sw,j}\frac{A_{sk,s}}{A_{sk,j}}Sw \cdot 2^{\frac{\Delta T_{sk,s}}{10}} \tag{35}$$

The Vasodilation and Vasoconstriction responses are convoluted, as both directly affect the perfusion in the skin blood vessels. The combined response of these two is described by Fiala et. al. [22] by

$$\beta'_{sk,s} = \frac{\beta'_{sk,0,s} + a_{dl,j} Dl}{1 + a_{cs,j} Cs \exp\left(-\frac{Dl}{80}\right)} \cdot 2^{\frac{\Delta T_{sk,s}}{10}} \tag{36}$$

Where $\beta'_{sk,0,s}$ is the de-facto blood perfusion rate factor at the skin node of sector s, and $a_{dl,j}$ and $a_{cs,j}$ are the distribution coefficients of element j for Vasodilation and Vasoconstriction respectively, and $\beta'_{sk,s}$ is the blood perfusion rate after accounting for Vasodilation and Vasoconstriction. The volume of blood available and not pumped to working muscles limits the maximum amount of vasodilation, as derived by Rowell [23] [24]. The new ceiling for the blood perfusion rate factor is

$$\beta'_{sk,\max} = 386.9 - 0.32 \mu H \tag{37}$$

Where $\mu = 0.932 K^{-1}$ and H is the total heat load due to work, from equation (20). This equation will be revisited, as volume limits to blood flow change drastically when the patient is undergoing hemorrhage.

Shock

A variety of variables change when the patient undergoes blood loss. For this study, the volume of blood in the patient undergoes a sharp drop over the course of 5 minutes, described by a blood pool volume drop of 40% [25] (Typical only to traumatic injuries [3]). In the model, this translates to a change in the final blood perfusion rate factor β_F before accounting for vasodilation and constriction. The new relation for β at time t is

$$\beta = \frac{V^{(t)}}{V_{IV,0}} \beta_F \tag{38}$$

The maximum skin perfusion rate factor $\beta'_{sk,\max}$ from (37) and the cardiac output variable CO in Table 4 in Appendix A are also scaled down by this volume ratio. It should be noted that the perfusion rate factor does not actually vary linearly with volume, as hypotension and the inelasticity of blood vessels form discrete limits. [26] These limits have not been accurately assessed [25] and as such they will be ignored, pending future research.

The above relation is the condition used for the cooling helmet. However, the ECMO machine can restore circulatory fluid volume despite not restoring blood via the addition of isotonic saline. Two variables, hematocrit and local tissue temperature, are used to characterize this system. The actual perfusion rate w_{bl} used to compute the perfusion rate factor β_F is given by [2]

$$w_{bl} = w_{bl,0} \bullet \alpha^{\beta(T-T_0)} \bullet \left(1 - \gamma \Delta_{HCT}\right) \tag{39}$$

Where $w_{bl,0}$ is the perfusion rate at thermal neutrality in $L \cdot s^{-1} \cdot m^{-3}$ (See Table 4 in Appendix A); α (-), β (K^{-1}), and γ (-) are constants derived from MATLAB's *fminunc* by Konstas et. al. [2]; and Δ_{HCT} is the change in hematocrit due to dilution, given by [2]

$$\Delta_{HCT} = \frac{p V_{RBC} \Delta V_{IV}}{V_{IV}\left(V_{IV} + p \Delta V_{IV}\right)} \tag{40}$$

Where $p = 0.33$ is a constant, ΔV_{IV} is the total added volume of saline, V_{IV} and V_{RBC} are the current total blood volume and red blood cell volume respectively, and $V_{RBC,0} = 2.1L$ and $V_{IV,0} = 5.0L$ are the red blood cell volume and total initial blood volume respectively.

The ECMO machine is simulated via a change in skin boundary conditions in the anterior thorax sector (See skin section) and an element-specific core blood pool temperature.

The core blood temperature for the elements downstream of the carotid artery (Head, neck, and face elements) is a design parameter for the heat exchanger, labeled T_{ECMO}. In this paper, as with the Tisherman trials [1], $T_{ECMO} = 10℃$. The outflow temperature of the ECMO machine is the driving cooling force for the brain; however, there are tissue cooling rate limits and local temperature bounds detailed in Xu et. al. [9] that prohibit T_{ECMO} from being set as low as possible. The density and specific heat capacities of the core blood pool in these elements are a weighted mixture of the outflow of the ECMO machine, derived from conservations of mass and energy as

$$\rho_{bl,p}^{(t)} = \frac{\left(\frac{V_{IV}^{(t)}}{V_{IV}^{(t)} + \Delta V_{IV}^{(t)}} \bullet Flow_{ECMO,blood}\right) \bullet \rho_{blood} + \left(\frac{\Delta V_{IV}^{(t)}}{V_{IV}^{(t)} + \Delta V_{IV}^{(t)}} \bullet Flow_{ECMO,blood} + Flow_{ECMO,saline}\right) \bullet \rho_{saline}}{Flow_{ECMO,blood} + Flow_{ECMO,saline}} \tag{41}$$

$$c_{P,bl,p}^{(t)} = \frac{\left(\frac{V_{IV}^{(t)}}{V_{IV}^{(t)} + \Delta V_{IV}^{(t)}} \bullet Flow_{ECMO,blood}\right) \rho_{blood} \bullet c_{P,blood} + \left(\frac{\Delta V_{IV}^{(t)}}{V_{IV}^{(t)} + \Delta V_{IV}^{(t)}} \bullet Flow_{ECMO,blood} + Flow_{ECMO,saline}\right) \rho_{saline} \bullet c_{P,saline}}{\left(\frac{V_{IV}^{(t)}}{V_{IV}^{(t)} + \Delta V_{IV}^{(t)}} \bullet Flow_{ECMO,blood}\right) \rho_{blood} + \left(\frac{\Delta V_{IV}^{(t)}}{V_{IV}^{(t)} + \Delta V_{IV}^{(t)}} \bullet Flow_{ECMO,blood} + Flow_{ECMO,saline}\right) \rho_{saline}} \tag{42}$$

This equation is applicable to both the saline and no-saline cases via the flexibility of the ECMO subscript. For pure saline injection, the ECMO subscript would indicate properties of isotonic saline. For a pure blood transfusion, the ECMO subscript would indicate properties of blood.

The variables $Flow_{ECMO}$ is the volumetric flow rate of the ECMO device ($\frac{m^3}{s}$), and is a design parameter of the device used. In the application in this paper, the volume of the central

blood pool is restored back to nominal via isotonic saline over a period dubbed recovery time t_{rec}. This relation gives

$$Flow_{ECMO,saline} = \frac{(V_{IV,0} - V_{IV,60\%})}{t_{rec}} \tag{43}$$

There is also a second component to $Flow_{ECMO}$, the recirculation of blood from the vena cava back into the carotid artery bifurcation while oxygenating the blood in the process. An important part of design for EPR would be selection of this predetermined value, since there are risks associated with both exceeding circulatory velocity during shock [10] and not providing enough oxygen to the patient. This second flow component $Flow_{ECMO,blood}$ is chosen to be from literature [2]

$$Flow_{ECMO,blood} = 250ml/min \bullet \frac{V_{IV} + \Delta V_{IV}}{V_{IV,0}} \tag{44}$$

Furthermore, over the rest of the body, the blood is assumed to be in quasi-equilibrium, meaning that the temperature difference between the current ECMO flow and the rest of the blood pool is completely mixed. At small timesteps rivaling the cardiac output, this assumption will fall apart. This leaves an averaging of the density, heat capacities, and temperatures as

$$\rho_{bl,p}^{(t+1)} = \frac{\left(V_{IV}{}^{(t)} + \Delta V_{IV}^{(t)}\right) \bullet \rho_{bl,p}^{(t)} + \left(Flow_{ECMO} \bullet \Delta t\right) \bullet \rho_{ECMO}^{(t)}}{\left(V_{IV}{}^{(t)} + \Delta V_{IV}^{(t)}\right) + \left(Flow_{ECMO} \bullet \Delta t\right)} \tag{45}$$

$$c_{P,bl,p}^{(t+1)} = \frac{\left(V_{IV}{}^{(t)} + \Delta V_{IV}^{(t)}\right) \rho_{bl,p}^{(t)} \bullet c_{P,bl,p}^{(t)} + \left(Flow_{ECMO} \bullet \Delta t\right) \rho_{ECMO}^{(t)} \bullet c_{P,ECMO}^{(t+1)}}{\left(V_{IV}{}^{(t)} + \Delta V_{IV}^{(t)}\right) \rho_{bl,p}^{(t)} + \left(Flow_{ECMO} \bullet \Delta t\right) \rho_{ECMO}^{(t)}} \tag{46}$$

$$\begin{aligned} \frac{T_{bl,p}^{(t+1)}}{T_{bl,p}^{(t)}} = & \frac{\left(V_{IV}{}^{(t)} + \Delta V_{IV}^{(t)}\right) \rho_{bl,p}^{(t)} c_{P,bl,p}^{(t)} \bullet T_{bl,p}^{(t)} + \left(Flow_{ECMO} \bullet \Delta t\right) \rho_{ECMO}^{(t)} c_{P,ECMO}^{(t)} \bullet T_{ECMO}^{(t)}}{\left(V_{IV}{}^{(t)} + \Delta V_{IV}^{(t)}\right) \rho_{bl,p}^{(t)} c_{P,bl,p}^{(t)} \bullet T_{bl,p}^{(t)}} \\ & \times \frac{\left(V_{IV}{}^{(t)} + \Delta V_{IV}^{(t)}\right) \rho_{bl,p}^{(t)} c_{P,bl,p}^{(t)}}{\left(V_{IV}{}^{(t)} + \Delta V_{IV}^{(t)}\right) \rho_{bl,p}^{(t)} c_{P,bl,p}^{(t)} + \left(Flow_{ECMO} \bullet \Delta t\right) \rho_{ECMO}^{(t)} c_{P,ECMO}^{(t)}} \end{aligned} \tag{47}$$

Notice how in equation (47) it seems like the next iteration of temperature is solved for. Rather, this is the ratio between the future and current temperatures in thermoneutrality; Other effects still convolute the result. However, this term appears in the equations for arterial blood temperature and the final equation for calculating $T_{bl,p}^{(t+1)}$ as a scalar multiplier.

The final blood perfusion rate β_r before vasodilation and vasoconstriction is given by a product of the above product solutions,

$$\beta_r^{(t)} = \rho_{bl,p}^{(t)} c_{P,bl,p}^{(t)} w_r^{(t)} \tag{48}$$

Skin

Skin Heat Flux

In the current model, two configurations are computed for skin and the skin boundary condition q_{sk}. In the first, the model is assumed to be clothed and in mixed natural and forced convection with the air. In the second, the model or parts of the model are placed in conductive contact with a cooling device; The second configuration is used in this study to simulate the cooling helmet from Diao [10].

The first configuration is detailed extensively in Fiala 1999 [13]. The skin heat flux q_{sk} is given by [13]

$$q_{sk} = q_c + q_R - q_{sR} + q_e \tag{49}$$

Where q_c is heat flux due to mixed convection, q_R is heat flux due to radiation on the body, q_{sR} is heat flux due to emission from the body, and q_e is heat flux due to evaporation.

q_c – Convection Heat Flux

Convection from the skin is described by the standard convection equation

$$q_c = h_{c,mix} \cdot \left(T_{sf} - T_{air}\right) \tag{50}$$

Where T_{sf} is the local skin surface temperature, T_{air} is the air temperature and $h_{c,mix}$ is given by

$$h_{c,mix} = \sqrt{a_{nat}\sqrt{T_{sf} - T_{air}} + a_{frc} \cdot v_{air,eff} + a_{mix}} \tag{51}$$

Where the skin parameters a_{nat}, a_{frc}, and a_{mix} are listed in Table 6 in Appendix A and $v_{air,eff}$ is the effective airspeed near the skin surface. This value may be modified to specific application [13], but an effective airspeed of $0.05 m/s$ was chosen for the sedentary subject.

q_R – Radiation Absorption Heat Flux

Radiation absorption is computed similarly as

$$q_R = h_R \cdot \left(T_{sf} - T_{sr,m}\right) \tag{52}$$

Where $T_{sr,m}$ is the mean surrounding temperature about the body and h_R is the radiation heat transfer coefficient, given as

$$h_R = \sigma \varepsilon_{sf} \varepsilon_{sr} \Psi_{sf-sr} \left(T*^2_{sf} + T*^2_{sr,m}\right)\left(T*_{sf} + T*_{sr,m}\right) \tag{53}$$

Where $\sigma = 5.67 \times 10^{-8} W \cdot m^{-2} \cdot K^{-4}$ is the Stefan-Boltzmann constant, ε_{sf} and ε_{sr} are the emission coefficients of the skin and surroundings respectively, Ψ_{sf-sr} is the view factor between the skin surface and the surroundings, and T^*_{sf} and T^*_{sr} are the absolute skin and surface temperatures in Kelvin. The view factors are functions of the patient's pose. View factors for the sedentary case and emission coefficients ε can be found in Table 6 of Appendix A. The problem parameters $T^*_{sr,m}$ and ε_{sr} are entirely dependent on the surroundings of the patient. The typical application of EPR suggests that the injury occurs outdoors, and then the patient is transported inside a closed vehicle whereupon the cooling device is applied. For this paper, the patient is assumed to be outdoors until cooling begins and then indoors. Problem parameters for the

outdoors and indoors scenarios are located in Table 2 in Appendix A. The changing surroundings also effect surrounding air temperatures, and are detailed in Table 2 in Appendix A.

q_{sR} – Radiation Emission Heat Flux

Emitted radiation is calculated as

$$q_{sR} = \alpha_{sf} \Psi_{sf-sr} s \tag{54}$$

Where α_{sf} is the surface absorption coefficient and s is the incident light intensity in W/m^2. Values for each are provided in Table 2 of Appendix A.

Clothing

Clothing has a substantial effect on resistances. Using a simplified version of the standard outfit offered by Oleson [27] changes the convective heat transfer coefficient in (51) and the radiation heat transfer coefficient in (53) into one lumped coefficient by the relation

$$U_{cl}^{*} = \frac{1}{n_j \cdot I_{cl}^{*} + \frac{1}{f_j^{*}\left(h_{c,mix} + h_R\right)}} \tag{55}$$

Where U_{cl}^{*} is the combined heat transfer coefficient through clothing in $W \cdot m^{-2}$, n_j is the equivalent number of layers of clothing applied, I_{cl}^{*} is a constant in $K \cdot m^2 \cdot W^{-1}$, and f_{cl}^{*} is 1 for unclothed elements and .9 for clothed elements. Values for I_{cl}^{*} and n_j can be found in Table 2 and Table 7 respectively in Appendix A.

The evaporative heat transfer is also changed by clothing layers, and is given by [13]

$$U_{e,cl}^{*} = \frac{L_{air}}{n_j \cdot \frac{I_{cl}^{*}}{i_{cl}^{*}} + \frac{1}{f_j^{*} \cdot h_{c,mix}}} \tag{56}$$

Where i_{cl}^{*} is given in Table 2 in Appendix A, and L_{air} is the Lewis constant for air $L_{air} = 0.0165\ K \cdot Pa^{-1}$. The coefficient U_{cl}^{*} controls heat flux due to pressure rather than temperature changes, in $W \cdot m^{-2} \cdot Pa^{-1}$.

q_e – Evaporation Heat Flux

Heat flux by evaporation is a complex computation of various variables, given as [13]

$$P_{osk,sat} = 100 \cdot \exp\left(18.956 - \frac{4030°C}{T_{sk} + 235°C}\right) \tag{57}$$

$$P_{sk} = \frac{\lambda_{H_2O}\frac{dm_{sw}}{A_{sk}dt} + \frac{P_{osk,sat}}{R_{e,sk}} + U_{e,cl}^{*}P_{air}}{U_{e,cl}^{*} + \frac{1}{R_{e,sk}}} \tag{58}$$

Where $P_{osk,sat}$ is the saturated vapor pressure in the outer skin and P_{sk} is the actual vapor pressure of the skin, both in Pa. T_{sk} is still the temperature at the skin boundary in °C, $\lambda_{H_2O} = 2{,}256\ kJ \cdot kg^{-1}$ is the latent heat of vaporization of water, A_{sk} is the area of the skin washer, $\frac{1}{R_{e,sk}} = 0.003\ W \cdot m^{-2} \cdot Pa^{-1}$ is the skin permeability, and P_{air} is given in Table 2 of Appendix A. The term $\frac{dm_{sw}}{dt}$ is given in the controlling system section of this paper.

The total evaporative heat flux is then given as

$$q_e = U_{e,cl}^{*} \cdot \left(P_{sk} - P_{air}\right) \tag{59}$$

Final Skin Heat Flux in mixed exposure

The final equation for skin heat flux is a modified version of (50), given as

$$q_{sk} = U_{cl}^{*}\left(T_{sk} - T_{weight}\right) + U_{e,cl}^{*}\left(P_{sk} - P_{air}\right) \tag{60}$$

Where T_{weigh} is

$$T_{weight} = \frac{h_{c,mix} T_{air} + h_R T_{sr,m} + q_{sR}}{h_{c,mix} + h_R} \tag{61}$$

Skin Heat Flux during External Cooling Device Application

Westin [14] created a framework for evaluating q_{sk} under application of an opaque cooling device like a dense helmet. The original application of Westin [14] was for forced liquid convective cooling, making it suitable for mobile heat exchanger cooling devices; However, minor modification also makes it applicable to conductive cooling devices like ice.

Assumptions are made about the nature of cooling devices. The incident light intensity s is assumed to be zero, negating q_{sR}. Assuming the patient and the device are in close contact, ε_{sr} approaches 1 and Ψ_{sf-sr} approaches 1. The nature of T_{sr} in the radiation term changes immensely depending on the device, but it will always be the temperature at the surface of the device in contact with the skin. It is assumed that in devices with conductive contact like heat exchanger pads and cooling helmets that T_{sr} is the film temperature $T_{sr} = T_f = \frac{1}{2}\left[T_{sk} + T_{fl}\right]$ where T_{fl} is the temperature of the working fluid; In devices with fluid exchange like an ECMO machine, T_{sr} is taken to be the temperature of the working fluid T_{fl}. Clothes are removed from the area of contact during external cooling, so n_j is assumed to be zero.

The skin heat flux then is an altered version of equation (49),

$$q_{sk} = q_c + q_R + q_e \tag{62}$$

Converting Heat Flux q_{sk} into a Finite Difference Equation

Skin has a fictional node representing the surroundings, similar to the treatment of non-homogenous node spacing in equation (10). The heat flux at the skin surface is equated to the conductive heat flux at the skin node via

$$q_{sk} = \frac{k_r \left(T_r - T_{(r+1)''} \right)}{r_{sk} \ln \left[\frac{r_{(r+1)''}}{r_r} \right]} \tag{63}$$

Solving this equation for $T_{(r+1)''}$ gives

$$T_{(r+1)''} = \frac{q_{sk} r_{sk}}{k_r} \ln \left[\frac{r_{(r+1)''}}{r_r} \right] + T_r \tag{64}$$

And this new fictional temperature node $T_{(r+1)''}$ can be directly substituted into equation (14).

VALIDATION

Thermoneutral Steady-State

The model was run with no cooling device in thermal neutrality for validation against the Fiala and modified Westin model. There are three stages for this computation. The first stage is creating a blank T0 vector with initial entries all at $307.55\ K$. The second stage is two iterations run with steady state equations. These can be obtained from equations (10), (12), and (14) by removing the current time solutions. The first iteration ignores the effects of parameters from timestep $(t-1)$ and the second iteration does not. These are the steady-state values with no transient computations and agree well with Westin [14]. The third stage is purely for transient validation, and is 100 iterations with a 1 second timestep with the transient form of the body matrix. Changes in the third stage are theoretically 0, and the infinity norm of the difference between stages 2 and 3 is $0.121K$.

Table 1 - Steady-State Thermoneutral Values

$T_{sk,m}$	$T_{bl,p}$	T_{hy}	ΣM
34.549℃	36.820℃	37.154℃	$72.755W$

Cooling Helmet – Diao Model

The model was run for the Diao [10] cooling helmet. All model runs are for 1 hour, 1 second timesteps. This case has shock, no ECMO flow, and no saline.

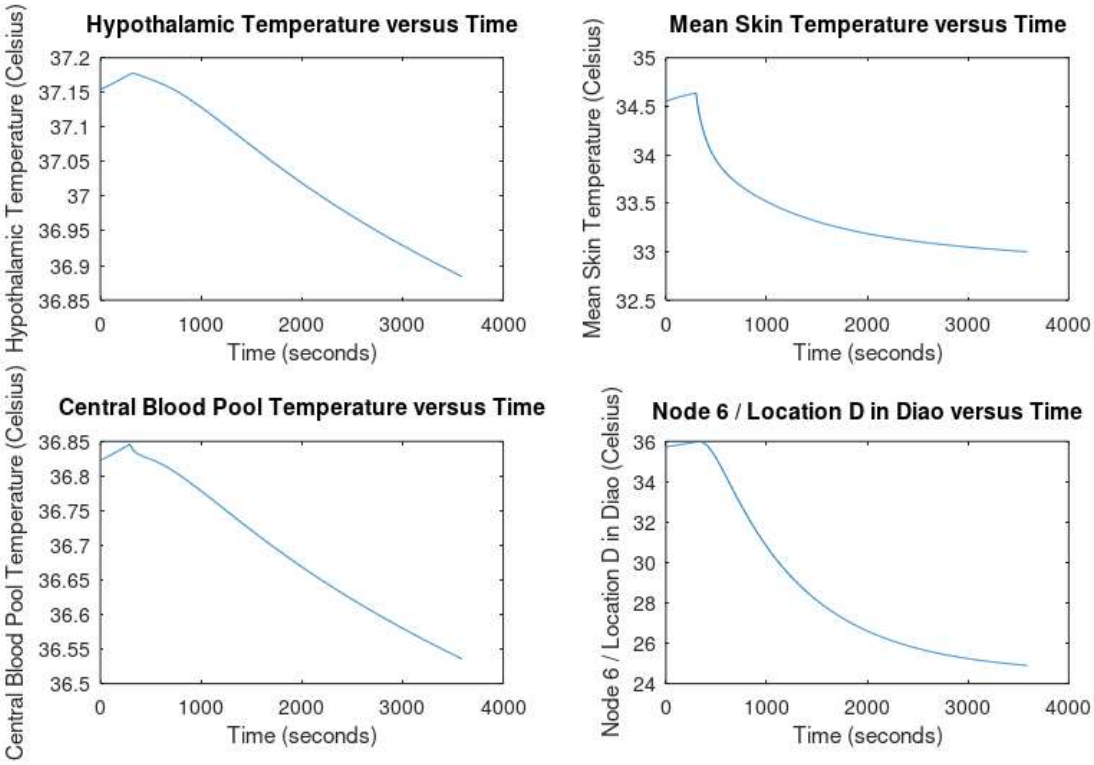

Figure 3 - Helmet Temperatures, Q_{10}=2

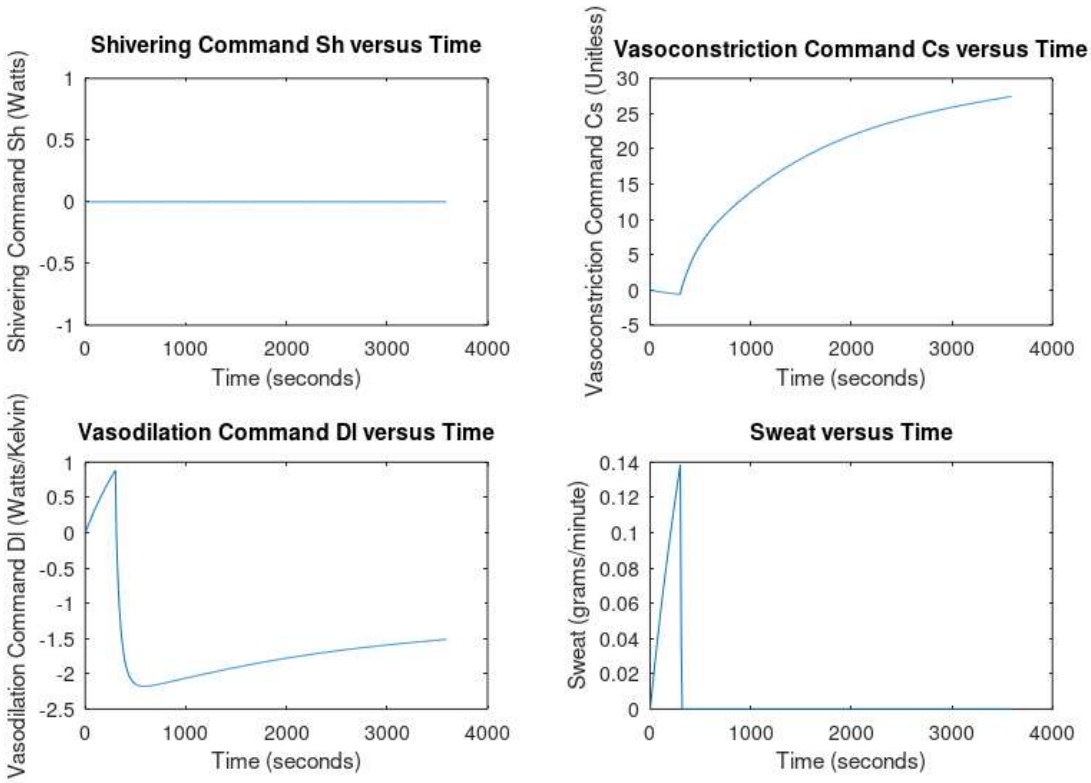

Figure 4 - Helmet Controls, Q_{10}=2

The fourth plot shown is the temperature measured at "Point D" on the Diao model, which is the ischemia condition at the inner surface of the skull. In the Fiala model, this is node 6.

In comparison to the Diao model, the plots have almost exactly the same shape but are scaled to the right about the initial time $t = t_{injury} = 300s$. This is likely because Diao uses $Q_{10} = 3$ throughout the paper, including scaling the blood perfusion rate. More recent papers use lower Q_{10} values. [15] [25] [14] When changing Q_{10} to 3 in this paper's Fiala model, the plot of point D matches Diao's and arrives at a similar final temperature: 24.901℃ vs Diao's 24.5℃. This paper's model achieves its final temperature later than that of Diao; Both Diao and this

model predict this: Modelling of whole-body heating means that the arterial temperature is not as impacted by changes in head temperatures.

ECMO Machine – No Saline

The ECMO machine described by Konstas [2] was implemented without a saline injection. Konstas [2] did not run this exact case, but results can be contrasted with the saline case.

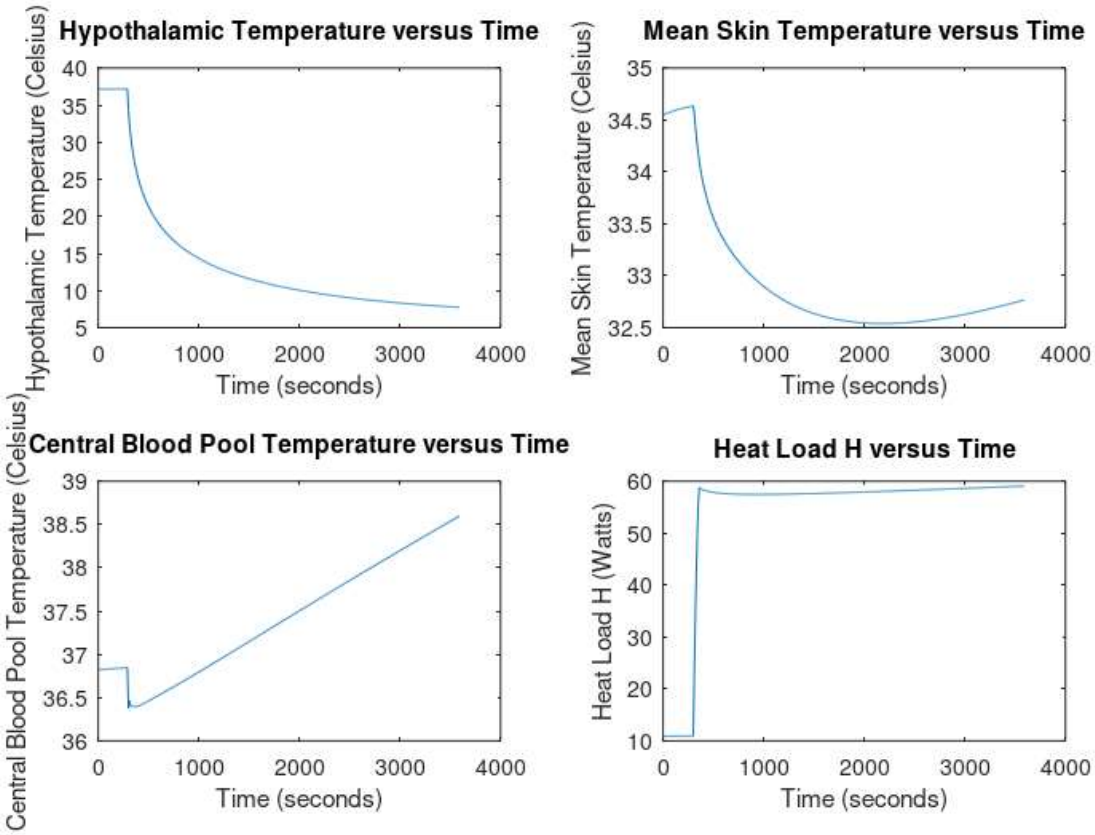

Figure 5 - ECMO Machine Temperatures, 5℃, no saline

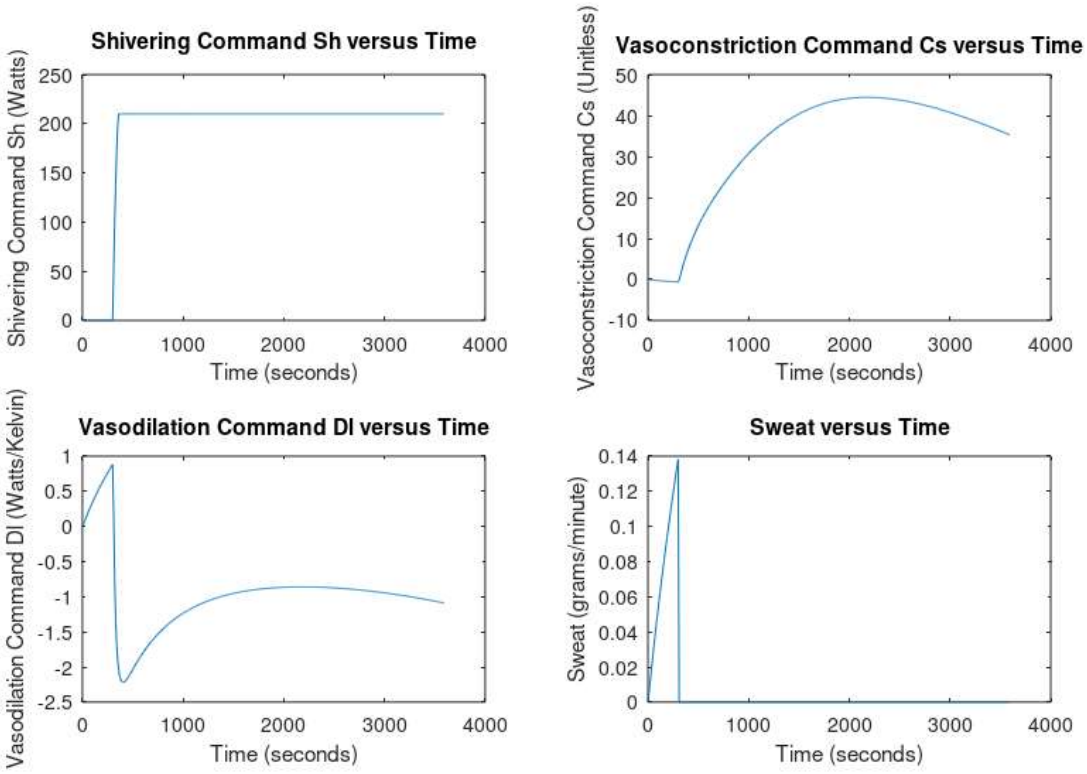

Figure 6 - ECMO Machine Controls, 5℃, no saline

The data shows a clear and sustained drop in the temperature of the central brain (Modeled by node 1). The temperature $T_{hy} = 10℃$ was achieved at 1717.8 seconds after initial ECMO machine application; roughly 28.63 minutes. This is an extremely optimistic result, as without pre-cooled saline to inject, the patient can undergo the requisite cooling within the 30 minute window offered by Tisherman [1]. The most notable apparent error in this formulation is the sharp spike in the shivering control, and the almost immediate drop in all temperatures. The discrete cusp in temperatures can be explained wholly by introduction of a new temperature in mixing contact with the existing blood pool. The spike in shivering, and the corresponding spike in heat load H, are consequences of the near-unlimited change in the ΔT_{hy} error signal.

ECMO Machine – Saline Injection

The ECMO machine was implemented, this time with a steady flow of isotonic saline over a predetermined 120 second time period after exsanguination until initial blood pool volume was restored.

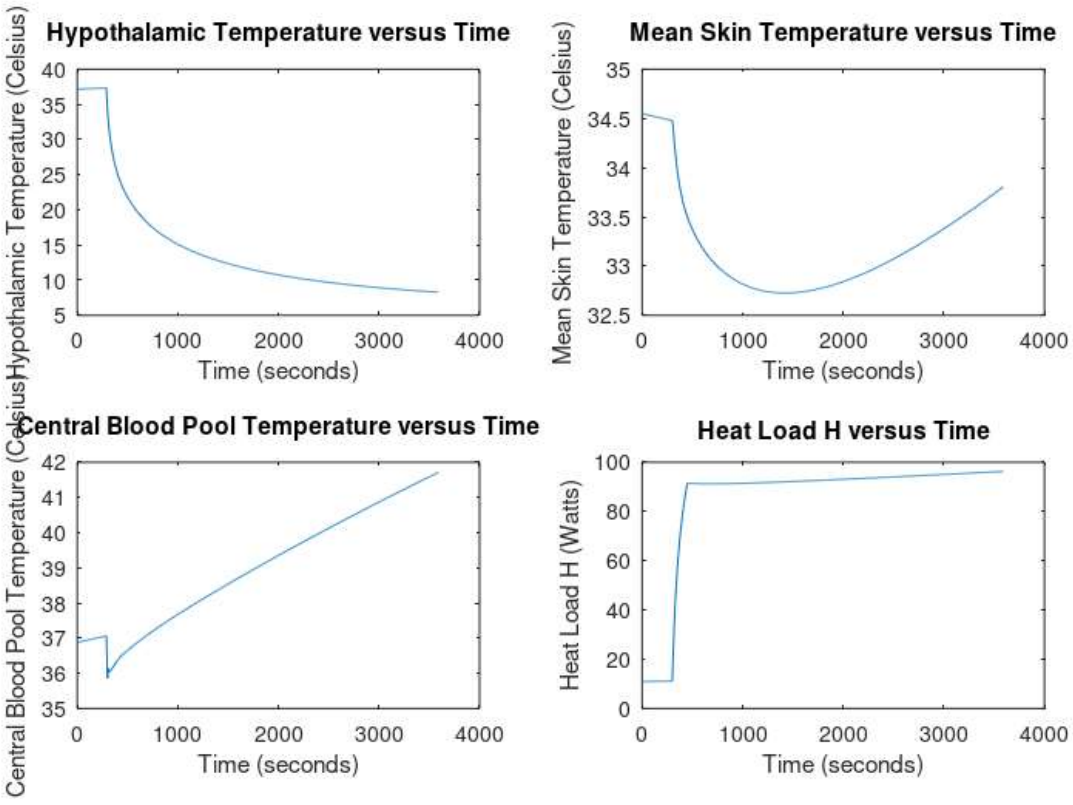

Figure 7 - ECMO Machine Temperatures, 5℃, saline

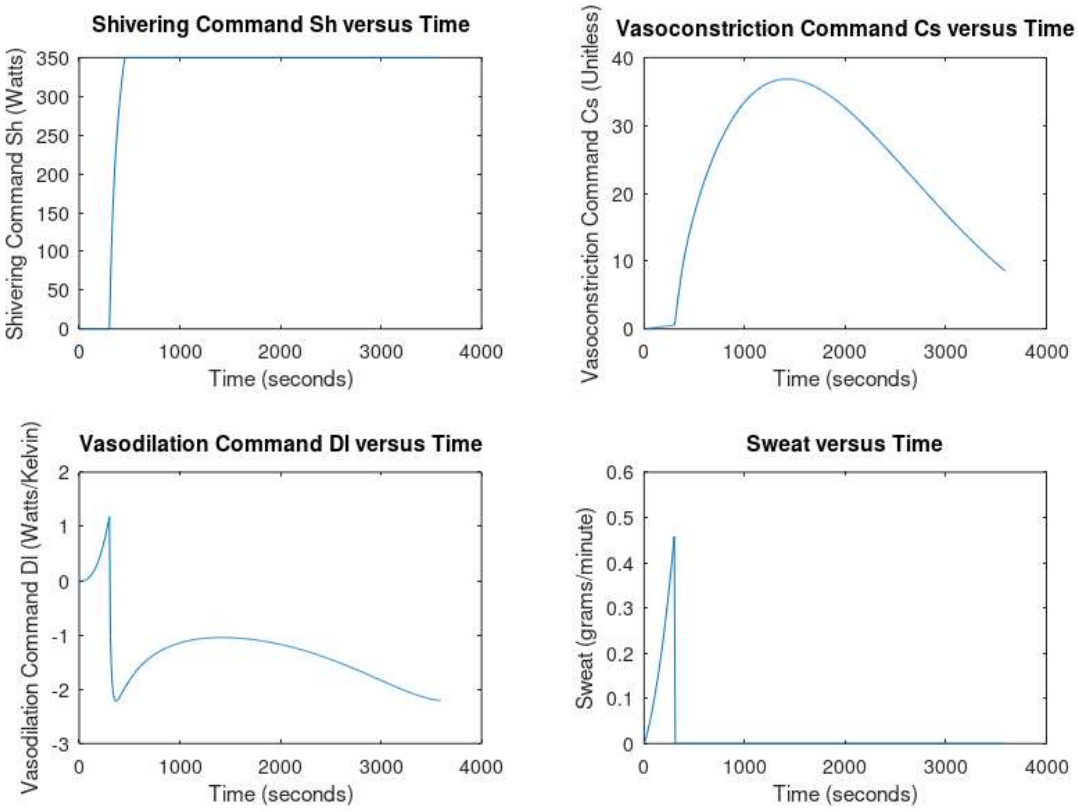

Figure 8 - ECMO Machine Controls, 5℃, saline

The saline case is meant to align with Konstas' saline injection case. It achieves temperature $T_{hy} = 10℃$ at time 2035.4 seconds after injury; roughly 33.9 minutes. The final temperature $T_{hy} = 7.902℃$ is also higher in this case versus the no-saline case. This is an interesting result: The initial rate of cooling for saline is higher than that of the non-saline option, but the achieved hypothalamic temperature is still higher. This is likely because the restoration of blood pool volume adds an extra load to be cooled by the ECMO machine; suggesting that there is a trade-off between speed of cooling and minimum final temperature.

The exact case from Konstas [2] is for a strict saline injection at 50 mL/min, at 1.8℃. This case can be replicated by resetting the blood temperature from ECMO outflow to core

blood, and having T_{saline} as 1.8℃. The two are mixed via the same heat capacity weighting as equation (47). Saline is injected until the volume is restored, resulting in a cusp around time $t = 2700$ seconds.

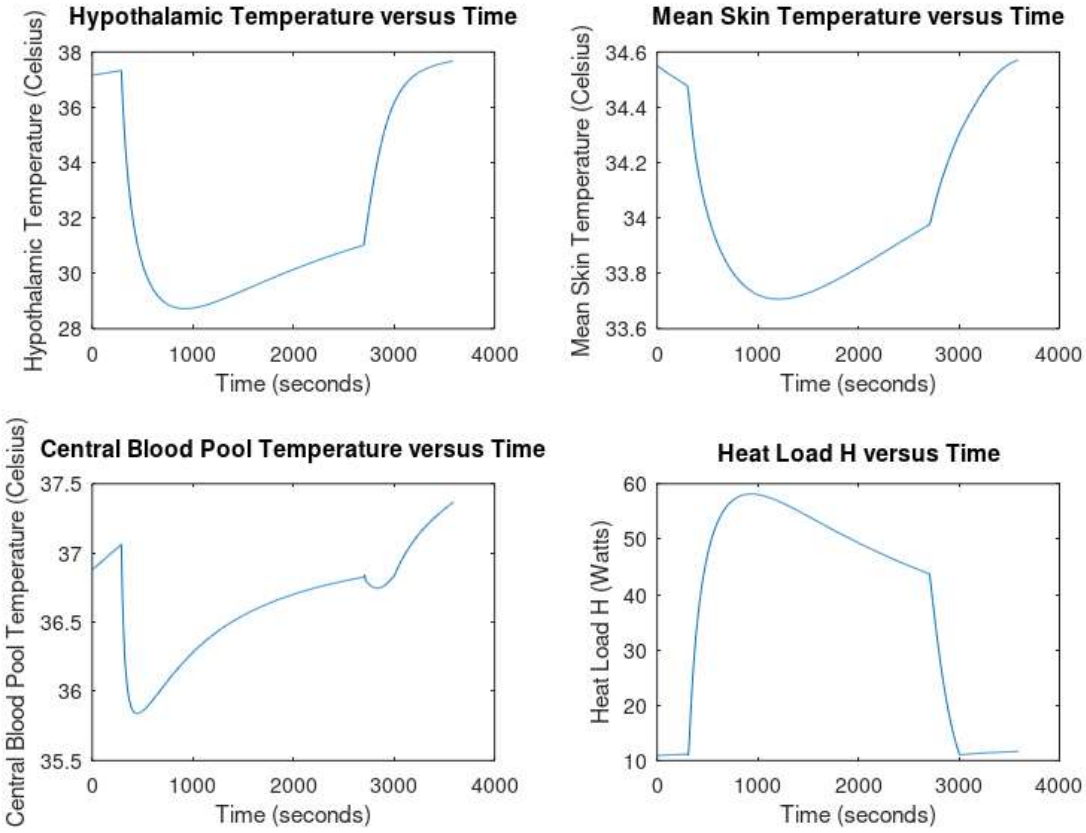

Figure 9 - Saline Injection Temperatures, no ECMO

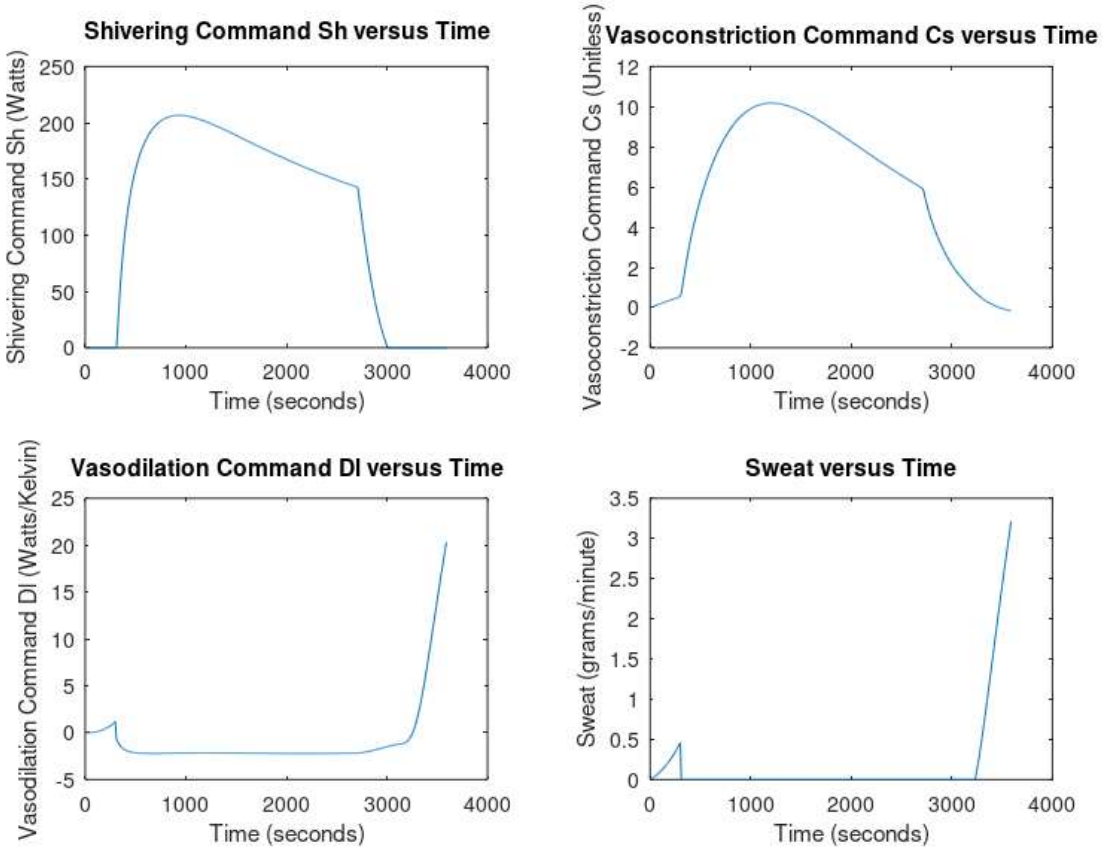

Figure 10 - Saline Injection Controls, no ECMO

This data matches extremely well with Konstas [2]. Konstas had a similar drop in hypothalamic temperature, down to a minimum value of 28.46℃ before rising up again. The minimum value achieved in this study was 28.725℃ . There was however a large difference between the rates of cooling in both models. This is likely because Konstas had accounted for the rate limit of tissue cooling, and scaled the saline temperature to never exceed this value. Beyond 10 minutes this rate is no longer a bounding limit, and faster cooling is maintained to reach 28.46℃.

CONCLUSIONS AND RECOMMENDATIONS

This new model is effectively three models stitched together, with new treatment of boundary conditions and ECMO flow. After validation from the Konstas and Diao cases, this model can be considered to have a high degree of accuracy and an improvement in terms of modelling ability over the two former models.

The element-based nature of this model means that body parts can be partially or fully removed to simulate traumatic injury with minimal effort. Capturing such an effect accurately requires intense speculation as to the nature of the injury; The countercurrent heat exchange coefficient h_x and the loss of blood at the point of injury are hard to quantify and even harder to find in literature.

This thesis only covers several boundary conditions: Fixed blood pool temperatures, fixed convection, and fixed blood and saline volumes. There are however more cases that can be tried in lieu of new cooling devices. The formulation of skin heat flux as a derived parameter makes it an easy condition to make fixed for a constant $\dot{q_{sk}}$. Contact-based devices like a cooling pad or ice could easily be modelled via a fixed $T_{sk''}$.

The primary improvement that could be made on this model is an improvement in fidelity at the brain. Modelling brain tissue with constant thermal parameters is not conducive to a study on brain temperatures. The next step would be switching to a finite-element model of the head, coupled via boundary conditions to the central blood pool and controlling signals. One such model is that of Dennis [28] which has been validated against a similar case as Diao's cooling helmet with abject success.

The second largest improvement would be a change to the shivering mechanism laid out in this paper. Westin [14] and Fanger [21] both derived shivering's error control as a power output to be executed by muscles throughout the body. During shock, deoxygenation and/or extreme hypothermia, this power output may be severely limited, a feature unaccounted for. Experimental qualitative data suggests that shivering reaches a cap and eventually subsides slightly as temperature decreases. [29] Shivering quickly becomes a driver of temperature increase in both the helmet and ECMO machine cases, so a more robust shivering control could have a large effect on final temperatures.

Future work on this model could include modelling oxygenation in tandem with tissue temperatures. This model is translated to practical results by comparing temperature-time profiles to those of clinical trials like Tisherman 2019 [1]. Successful cases dictate the maximal cooling rates and maximum times until sufficient induced hypothermia where the patient will survive; which means only that noticeable permanent damage has either occurred or not occurred. Damage due to deoxygenation, however, is a very complex function of metabolism and becomes uncoupled from temperature at low values. [30]

APPENDICES

APPENDIX A – PARAMETERS OF FIALA MODEL

The Fiala model used in this study is for a sedentary person, undergoing low activity.

Table 2 - Parameters for Body Model [13] [14] [21] [31] [32]

Parameter	Value
$M_{bas,ref}$	$87\ \mathrm{W/m^3}$
$M_{bas,0}$	$58.2\ \mathrm{W/m^3}$
act_{bas}	0.8 met
b_1	$.39\ \mathrm{met^{-1}}$
b_0	$-.60$
T_{ENV}	26℃
η_w	20%
$v_{air,eff}$	$0.05\ m/s$
$T_{air,outdoors}$	26℃
$T_{air,indoors}$	22℃
$T^*_{sr,m,outdoors}$	$T_{air,outdoors}$
$T^*_{sr,m,indoors}$	$T_{air,indoors}$
$\varepsilon_{sr,outdoor}$	0.46
$\varepsilon_{sr,indoor}$	0.93
$\alpha_{sr,indoor}$	0.8
s_{indoor}	500 lux
$\alpha_{sr,outdoor}$	0.3
$s_{outdoor}$	10752 lux

I_{cl}^{*}	$0.093 W m^{-2} K^{-1}$
i_{cl}^{*}	0.34
P_{air}	2.3 kPa
ρ_{saline}	$1004.6 kg \cdot m^{-3}$
ρ_{blood}	$1069 kg \cdot m^{-3}$
$c_{P,saline}$	$4180 J \cdot kg^{-1} K^{-1}$
$c_{P,blood}$	$3650 J \cdot kg^{-1} K^{-1}$

Table 3 - Geometrical Parameters of Fiala Model [13]

Element	Shape	Length (cm)	Sectors	ϕ (°)	Tissue	# Nodes	r_0 (cm)
Head	Partial Sphere	N.A.	Forehead	10	Brain	5	8.60
			Head	170	Bone	2	10.05
					Fat	2	10.20
					Skin	4	10.40
Face	Partial Cylinder	9.84		210	Muscle	1	2.68
					Bone	1	5.42
					Muscle	1	6.80
					Fat	2	7.60
					Skin	2	7.80
Neck	Cylinder	8.42	Anterior	180	Bone	1	1.90
			Posterior	180	Muscle	4	5.46
					Fat	2	5.56
					Skin	4	5.67
Shoulders	Partial Cylinder	32		130	Bone	1	3.70
					Muscle	2	3.90
					Fat	2	4.40
					Skin	2	4.60
Thorax	Cylinder	30.6	Anterior	150	Lung	1	7.73
			Posterior	150	Bone	3	8.91
			Inferior	60	Muscle	3	12.34
					Fat	6	12.68
					Skin	6	12.90
Abdomen	Cylinder	55.2	Anterior	150	Viscera	1	7.85
			Posterior	150	Bone	3	8.34
			Inferior	60	Muscle	3	10.90
					Fat	6	12.44
					Skin	6	12.60
Arms	Cylinder	127.4	Anterior	135	Bone	1	1.53
			Posterior	135	Muscle	3	3.43
			Inferior	90	Fat	6	4.01
					Skin	6	4.18
Hands	Cylinder	62	Back	180	Bone	1	0.70
			Palm	180	Muscle	2	1.74
					Fat	2	2.04
					Skin	4	2.26
Legs	Cylinder	139	Anterior	150	Bone	1	2.20
			Posterior	150	Muscle	6	4.80
			Inferior	60	Fat	6	5.33
					Skin	6	5.53
Feet	Cylinder	48	Instep	180	Bone	1	2.00
			Sole	180	Muscle	2	2.50
					Fat	4	3.26
					Skin	4	3.50

Table 4 - Fiala Model Tissue Parameters [13]

Element	h_x (WK^{-1})	Tissue	k $(\frac{W}{m \cdot K})$	ρ $(\frac{kg}{m^3})$	c $(\frac{J}{kg \cdot K})$	$w_{bl,0}$ $(L\,s^{-1}m^{-3})$	$q_{m,0}$ $(W\,m^{-3})$
Head	0	Brain	0.49	1080	3850	10.1320	13400
		Bone	1.16	1500	1591	0.0000	0
		Fat	0.16	850	2300	0.0036	58
		Skin	0.47	1085	3680	5.4800	368
Face	0	Muscle	0.42	1085	3768	0.5380	684
		Bone	1.16	1500	1591	0.0000	0
		Muscle	0.42	1085	3768	0.5380	684
		Fat	0.16	850	2300	0.0036	58
		Skin	0.47	1085	3680	11.1700	368
Neck	0	Bone	0.75	1357	1700	0.0000	0
		Muscle	0.42	1085	3768	0.5380	684
		Fat	0.16	850	2300	0.0036	58
		Skin	0.47	1085	3680	6.8000	368
Shoulders	0.8	Bone	0.75	1357	1700	0.0000	0
		Muscle	0.42	1085	3768	0.5380	684
		Fat	0.16	850	2300	0.0036	58
		Skin	0.47	1085	3680	1.0100	368
Thorax	0	Lung	0.28	550	3718	CO	600
		Bone	0.75	1357	1700	0.0000	0
		Muscle	0.42	1085	3768	0.5380	684
		Fat	0.16	850	2300	0.0036	58
		Skin	0.47	1085	3680	1.5800	368
Abdomen	0	Viscera	0.53	1000	3697	4.3100	4100
		Bone	0.75	1357	1700	0.0000	0
		Muscle	0.42	1085	3768	0.5380	684
		Fat	0.16	850	2300	0.0036	58
		Skin	0.47	1085	3680	1.4400	368
Arms	4.13	Bone	0.75	1357	1700	0.0000	0
		Muscle	0.42	1085	3768	0.5380	684
		Fat	0.16	850	2300	0.0036	58
		Skin	0.47	1085	3680	1.1000	368
Hands	0.57	Bone	0.75	1357	1700	0.0000	0
		Muscle	0.42	1085	3768	0.5380	684
		Fat	0.16	850	2300	0.0036	58
		Skin	0.47	1085	3680	4.5400	368
Legs	6.9	Bone	0.75	1357	1700	0.0000	0
		Muscle	0.42	1085	3768	0.5380	684
		Fat	0.16	850	2300	0.0036	58
		Skin	0.47	1085	3680	1.0500	368
Feet	3.4	Bone	0.75	1357	1700	0.0000	0
		Muscle	0.42	1085	3768	0.5380	684
		Fat	0.16	850	2300	0.0036	58
		Skin	0.47	1085	3680	1.5000	368
Blood				1069	3650		

Table 5 - Distribution Parameters (a) [13] [22]

Element	$a_{m,w}$	a_{sw}	a_{dl}	a_{cs}	a_{sh}
Head	0.00	0.095	0.055	0.0300	0.0000
Face	0.00	0.054	0.046	0.0330	0.0020
Neck	0.03	0.042	0.031	0.0250	0.0020
Shoulders	0.05	0.037	0.020	0.0100	0.0002
Thorax	0.12	0.101	0.141	0.0005	0.6305
Abdomen	0.46	0.181	0.161	0.0205	0.2400
Arms	0.19	0.133	0.095	0.1945	0.0400
Hands	0.02	0.049	0.121	0.1100	0.0020
Legs	0.11	0.261	0.230	0.2000	0.0813
Feet	0.02	0.047	0.100	0.3765	0.0020

Table 6 - Exposed Skin Parameters [13]

	$h_{c,mix}$					View Factor	Emission Coefficient
Element	a_{nat}	a_{frc}	a_{mix}	a_{sk}	**Sector**	Ψ_{sf-sr}	ε
Head	3	113	-5.70	0.08350	Forehead	1.00	0.99
					Head	0.90	0.80
Face	3	113	-5.70	0.04180		0.90	0.99
Neck	1.6	130	-6.50	0.04170	Anterior	0.70	0.99
					Posterior	0.75	0.99
Shoulders	5.9	216	-10.80	0.03000		0.90	0.99
Thorax	0.5	180	-7.40	0.30600	Anterior	0.80	0.99
					Posterior	0.95	0.99
					Inferior	0.05	0.99
Abdomen	0.5	180	-9.00	0.12100	Anterior	0.80	0.99
					Posterior	0.95	0.99
					Inferior	0.20	0.99
Arms	8.3	216	-10.80	0.18000	Anterior	0.75	0.99
					Posterior	0.80	0.99
					Inferior	0.10	0.99
Hands	8.3	216	-10.80	0.09000	Handback	0.80	0.99
					Palm	0.10	0.99
Legs	5.3	220	-11.00	0.20800	Anterior	0.85	0.99
					Posterior	0.95	0.99
					Inferior	0.10	0.99
Feet	5.3	220	-11.00	0.07500	Instep	0.90	0.99
					Sole	1.00	0.99

Table 7 - Clothing Parameters

Element	n_j
Head	0
Face	0
Neck	0
Shoulders	1
Thorax	1
Abdomen	1
Arms	0
Hands	0
Legs	1
Feet	3

APPENDIX B – ADVANCED GEOMETRICAL PARAMETERS

Advanced geometrical parameters are detailed here.

Conduction Parameter A

Cylinder - Backwards Case

$$A_{B,r,cyl} = \frac{D_{B,r-1,cyl}\Lambda_{B,r,cyl} - Ds_{B,r,cyl}\Lambda_{B,r-1,cyl}}{D_{B,r-1,cyl}\Lambda_{B,r,cyl} - D_{B,r,cyl}\Lambda_{B,r-1,cyl}} \tag{0.65}$$

$$A_{B,r-1,cyl} = \frac{\Lambda_{B,r-1,cyl}}{D_{B,r-1,cyl}\Lambda_{B,r,cyl} - D_{B,r,cyl}\Lambda_{B,r-1,cyl}} \tag{0.66}$$

Where

$$\Lambda_{B,r,cyl} = \frac{k_r}{\ln\left(\frac{r_r}{r_r - \Delta r_r}\right)} \tag{0.67}$$

$$\Lambda_{B,r-1,cyl} = \frac{k_{r-1}}{\ln\left(\frac{r_{r-1} + \Delta r_{r-1}}{r_{r-1}}\right)} \tag{0.68}$$

$$D_{B,r,cyl} = \frac{\ln\left(\frac{r_{ifc}}{r_r}\right)}{\ln\left(\frac{r_r}{r_r - \Delta r_r}\right)} \tag{0.69}$$

$$Ds_{B,r,cyl} = \frac{\ln\left(\frac{r_{ifc}}{r_r - \Delta r_r}\right)}{\ln\left(\frac{r_r}{r_r - \Delta r_r}\right)} \tag{0.70}$$

Cylinder – Forwards Case

$$A_{F,r,cyl} = \frac{Ds_{F,r,cyl}\Lambda_{F,r+1,cyl} - D_{F,r+1,cyl}\Lambda_{F,r,cyl}}{D_{F,r,cyl}\Lambda_{F,r+1,cyl} - D_{F,r+1,cyl}\Lambda_{F,r,cyl}} \tag{0.71}$$

$$A_{F,r+1,cyl} = \frac{\Lambda_{F,r+1,cyl}}{D_{F,r,cyl}\Lambda_{F,r+1,cyl} - D_{F,r+1,cyl}\Lambda_{F,r,cyl}} \tag{0.72}$$

Where

$$\Lambda_{F,r,cyl} = \frac{k_r}{\ln\left(\frac{r_r + \Delta r_r}{r_r}\right)} \tag{0.73}$$

$$\Lambda_{F,r+1,cyl} = \frac{k_{r+1}}{\ln\left(\frac{r_{r+1}}{r_{r+1} - \Delta r_{r+1}}\right)} \tag{0.74}$$

$$D_{F,r,cyl} = \frac{\ln\left(\frac{r_{ifc}}{r_r}\right)}{\ln\left(\frac{r_r + \Delta r_r}{r_r}\right)} \tag{0.75}$$

$$Ds_{F,r,cyl} = \frac{\ln\left(\frac{r_{ifc}}{r_r + \Delta r_r}\right)}{\ln\left(\frac{r_r + \Delta r_r}{r_r}\right)} \tag{0.76}$$

$$D_{F,r+1,cyl} = \frac{\ln\left(\frac{r_{ifc}}{r_{r+1}}\right)}{\ln\left(\frac{r_{r+1}}{r_{r+1} - \Delta r_{r+1}}\right)} \tag{0.77}$$

Spherical – Backwards Case

$$A_{B,r,sph} = \frac{\Lambda_{B,r,sph} - \Lambda_{B,r-1,sph}\frac{r_r}{r_{r-1} + \Delta r_{r-1}}}{\Lambda_{B,r,sph} + \Lambda_{B,r-1,sph}\frac{r_r - \Delta r_r}{r_{r-1} + \Delta r_{r-1}}} \tag{0.78}$$

$$A_{B,r-1,sph} = \frac{\Lambda_{B,r-1,sph}\left(1 + \frac{r_{r-1}}{r_{r-1} + \Delta r_{r-1}}\right)}{\Lambda_{B,r,sph} + \Lambda_{B,r-1,sph}\frac{r_r - \Delta r_r}{r_{r-1} + \Delta r_{r-1}}} \tag{0.79}$$

Where

$$\Lambda_{B,r,sph} = \frac{k_r}{\frac{1}{r_r - \Delta r_r} - \frac{1}{r_r}} \tag{0.80}$$

$$\Lambda_{B,r-1,sph} = \frac{k_{r-1}}{\frac{1}{r_{r-1}} - \frac{1}{r_{r-1} + \Delta r_{r-1}}} \tag{0.81}$$

Spherical – Forwards Case

$$A_{F,r,sph} = \frac{\Lambda_{F,r,sph} - \Lambda_{F,r+1,sph} \frac{r_r}{r_{r+1} - \Delta r_{r+1}}}{\Lambda_{F,r,sph} + \Lambda_{F,r+1,sph} \frac{r_r + \Delta r_r}{r_{r+1} - \Delta r_{r+1}}} \tag{0.82}$$

$$A_{F,r+1,sph} = \frac{\Lambda_{F,r+1,sph} \left(1 + \frac{r_{r+1}}{r_{r+1} - \Delta r_{r+1}}\right)}{\Lambda_{F,r,sph} + \Lambda_{F,r+1,sph} \frac{r_r + \Delta r_r}{r_{r+1} - \Delta r_{r+1}}} \tag{0.83}$$

Where

$$\Lambda_{F,r,sph} = \frac{k_r}{\frac{1}{r_r} - \frac{1}{r_r + \Delta r_r}} \tag{0.84}$$

$$\Lambda_{F,r+1,sph} = \frac{k_{r+1}}{\frac{1}{r_{r+1} - \Delta r_{r+1}} - \frac{1}{r_{r+1}}} \tag{0.85}$$

Isothermal Core Parameter θ

Cylinder Case

$$\theta_{cyl} = \frac{8\left(1 - \frac{1}{\sqrt{2}}\right)^2}{\ln\left(2\sqrt{2} - 1\right) \sum_{s}^{\text{sectors}} \phi_s} \tag{0.86}$$

Spherical Case

$$\theta_{sph} = \frac{12\left(\sqrt[3]{16}-1\right)\left(1-\frac{1}{\sqrt[3]{2}}\right)^2}{\left(\sqrt[3]{32}-\sqrt[3]{16}\right)\sum_{s}^{\text{sectors}}\phi_s} \tag{0.87}$$

LIST OF REFERENCES

[1] S. A. Tisherman, M. E. Kutcher and R. M. Forsythe, "Emergency preservation and resuscitation for cardiac arrest from trauma," *International Journal of Surgery,* vol. 33B, pp. 209-212, 2016.

[2] A.-A. Konstas, M. A. Neimark, A. F. Laine and J. Pile-Spellman, "A theoretical model of selective cooling using intracarotid cold saline infusion in the human brain," *Journal of Applied Physiology,* vol. 102, no. 4, pp. 1329-1340, 2007.

[3] S. Taghavi and R. Askari, "Hypovolemic Shock," StatPearls Publishing, Treasure Island, FL, 2020.

[4] D. Trunkey, "Accidental and intentional injuries account for more years of life lost in the U.S. than cancer and heart disease. Among the prescribed remedies are improved preventive efforts, speedier surgery and further research.," *Scientific American,* vol. 249, no. 2, pp. 28-35, 1983.

[5] L. D. Procter, "Intravenous Fluid Resuscitation," October 2020. [Online]. Available: https://www.merckmanuals.com/professional/critical-care-medicine/shock-and-fluid-resuscitation/intravenous-fluid-resuscitation. [Accessed 25 March 2021].

[6] Military Times, "Study: 25% of war deaths medically preventable," Military Times, 29 March 2013. [Online]. Available: https://www.militarytimes.com/2013/03/29/study-25-of-war-deaths-medically-

preventable/#:~:text=A%20new%20study%20finds%20that,have%20had%20a%20fighting%20chance.. [Accessed 28 February 2021].

[7] E. Kagawa, "Extracorporeal cardiopulmonary resuscitation for adult cardiac arrest patients," *World Journal of Critical Care Medicine,* vol. 1, no. 2, pp. 46-49, 2012.

[8] X. Xu, P. Tikuisis and G. Giesbrecht, "A mathematical model for human brain cooling during cold-water near-drowning.," *Journal of Applied Physiology,* vol. 86, no. 1, pp. 265-272, 1999.

[9] X. Xu and P. Tikuisis, "Thermoregulatory Modeling for Cold Stress," *Comprehensive Physiology,* vol. 4, pp. 1057-1081, 2014.

[10] C. Diao, L. Zhu and H. Wang, "Cooling and Rewarming for Brain Ischemia or Injury: Theoretical Analysis," *Annals of Biomedical Engineering,* vol. 31, pp. 346-353, 2003.

[11] S. A. Tisherman, "Suspended Animation for Resuscitation from Exsanguinating Hemorrhage," *Critical Care Medicine,* vol. 32, 2004.

[12] H. Thomson, "Exclusive: Humans placed in suspended animation for the first time," New Scientist Ltd., 20 November 2019. [Online]. Available: https://www.newscientist.com/article/2224004-exclusive-humans-placed-in-suspended-animation-for-the-first-time/. [Accessed 20 February 2021].

[13] D. Fiala, K. J. Lomas and M. Stohrer, "A computer model of human thermoregulation for a wide range of environmental conditions: the passive system," *Journal of Applied Physiology,* vol. 87, no. 5, 1999.

[14] J. Westin, "An Improved Thermoregulatory Model For Cooling Garment Applications With Transient Metabolic Rates," *STARS Electronic Theses and Dissertations,* no. 3704, 2008.

[15] D. Fiala, G. Havenith, P. Bröde, B. Kampmann and G. Jendritzky, "UTCI-Fiala multi-node model of human heat transfer," *International Journal of Biometeorology,* vol. 56, pp. 429-441, 2012.

[16] H. H. Pennes, "Analysis of Tissue and Arterial Blood Temperatures in the Resting Human Forearm," *Journal of Applied Physiology,* vol. 1, pp. 93-122, 1948.

[17] J. A. J. Stolwijk, "A Mathematical Model of Physiological Temperature Regulation in Man," *NASA Technical Reports,* vol. 1855, 1971.

[18] E. H. Wissler, "A Mathematical Model of the Human Thermal System," *Bulletin of Mathematical Biophysics,* vol. 26, pp. 147-166, 1964.

[19] F. Kim, M. Olsufka, W. J. Longstreth, C. Maynard, D. Carlbom, S. Deem, P. Kudenchuk, M. Copass and L. Cobb, "Pilot randomized clinical trial of prehospital induction of mild hypothermia in out-of-hospital cardiac arrest patients with a rapid infusion of 4 degrees C normal saline," *Circulation,* vol. 115, no. 24, pp. 3064-3070, 2007.

[20] N. T. Kouchoukos and J. W. Kirklin, Kirklin/Barratt-Boyes cardiac surgery : morphology, diagnostic criteria, natural history, techniques, results, and indications., Philadelphia: Elsevier/Saunders, 2013.

[21] P. O. Fanger, "Thermal comfort: Analysis and applications in environmental engineering," Danish Technical Press, Copenhagen, 1970.

[22] D. Fiala, K. Lomas and M. Stohrer, "Computer prediction of human thermoregulatory and temperature responses to a wide range of environmental conditions," *International Journal of Biometeorology,* vol. 45, pp. 143-159, 2001.

[23] L. Rowell, "Human cardiovascular adjustments to exercise and thermal stress.," *Physiology Review,* vol. 54, pp. 75-159, 1974.

[24] J. L. Johnson, G. L. Brengelmann and L. B. Rowell, "Modification of the skin blood flow - body temperature relationship by upright exercise.," *Journal of Applied Physiology,* vol. 37, pp. 880-886, 1974.

[25] A. Fülöp, Z. Turóczi, D. Garbaisz, L. Harsányi and A. Szijártó, "Experimental Models of Hemorrhagic Shock: A Review," *Eur Surg Res,* vol. 50, pp. 57-70, 2013.

[26] J. L. Gainer, M. J. Lipa and M. C. Ficenec, "Hemorrhagic shock in rats," *Laboratory animal science,* vol. 45, no. 2, pp. 169-172, 1995.

[27] B. W. Oleson and P. O. Fanger, "The skin temperature distribution for resting man in comfort," *Archives of Scientific Physiology,* vol. 27, pp. A385-A393, 1973.

[28] B. H. Dennis, R. C. Eberhart, G. S. Dulikravich and S. W. Radons, "Finite-Element Simulation of Cooling of Realistic 3-D Human Head and Neck," *Transactions of the ASME,* vol. 125, pp. 832-840, 2003.

[29] R. Lakshmanan, F. Sadaka and A. Palagiri, "Therapeutic Hypothermia: Adverse Events, Recognition, Prevention and Treatment Strategies," in *Therapeutic Hypothermia in Brain Injury*, IntechOpen, 2013.

[30] M. P. Ehrlich, J. N. McCullough, N. Zhang, D. J. Weiss, T. Juvonen, C. A. Bodian and R. B. Griepp, "Effect of hypothermia on cerebral blood flow and metabolism in the pig," *Annals of Thoracic Surgery,* vol. 73, pp. 191-197, 2002.

[31] Engineering Toolbox, "Surface - Radiation Absorptivity," Engineering Toolbox, 2011. [Online]. Available: https://www.engineeringtoolbox.com/radiation-surface-absorptivity-d_1805.html. [Accessed 04 March 2021].

[32] Engineering Toolbox, "Illuminance - Recommended Light Level," Engineering Toolbox, 2004. [Online]. Available: https://www.engineeringtoolbox.com/light-level-rooms-d_708.html. [Accessed 04 March 2021].